ACR No. L5A03

NATIONAL ADVISORY COMMITTEE FOR AERONAUTICS

WARTIME REPORT

ORIGINALLY ISSUED

January 1945 as
Advance Confidential Report L5A03

EXPERIMENTAL VERIFICATION OF A SIMPLIFIED VEE-TAIL THEORY AND ANALYSIS OF AVAILABLE DATA ON COMPLETE MODELS WITH VEE TAILS

By Paul E. Purser and John P. Campbell

Langley Memorial Aeronautical Laboratory
Langley Field, Va.

NACA

WASHINGTON

NACA ACR No. L5A03 [redacted]

NATIONAL ADVISORY COMMITTEE FOR AERONAUTICS

ADVANCE CONFIDENTIAL REPORT

EXPERIMENTAL VERIFICATION OF A SIMPLIFIED VEE-TAIL THEORY AND ANALYSIS OF AVAILABLE DATA ON COMPLETE MODELS WITH VEE TAILS

By Paul E. Purser and John P. Campbell

SUMMARY

An analysis has been made of available data on vee-tail surfaces. Previously published theoretical studies of vee tails have been extended to include the control effectiveness and control forces in addition to the stability. Tests of two isolated tail surfaces with various amounts of dihedral provided a check of the theory. Methods for designing vee tails were also developed and are given in the present paper.

The analysis indicated that a vee tail designed to provide values of stability and control parameters equal to those provided by a conventional tail would probably provide no reduction in area unless the conventional vertical tail is in a bad canopy wake or unless the vee tail has a higher effective aspect ratio than the conventional vertical and horizontal tails.

The analysis also indicated that a possible reduction in control forces (or in the amount of control balance required) can be made by the use of a vee tail, provided large deflections of the control surface do not cause a large decrease in the effectiveness and increase in hinge-moment coefficient per degree deflection of the control surface. If large-chord control surfaces must be used in order to keep the control deflections small, the control forces (or the amount of control balance required) on the vee tail are likely to be equal to or greater than those for the conventional tail assembly.

The analysis further indicated that the vee tail could have the following advantages over the conventional tail assembly:

[redacted]

(1) Less drag because the vee tail has fewer fuselage-tail junctures

(2) Less tendency toward rudder lock

(3) Higher location of tail surfaces, which tends to reduce elevator deflection required for take-off and landing, to keep the tail out of spray in flying-boat take-off, and to reduce possibilities of tail buffeting from the wing and canopy wakes in high-speed flight

(4) Fewer tail surfaces to manufacture

On the other hand, the analysis indicated the following disadvantages that a vee tail might have when compared with conventional tails:

(1) Possible interaction of elevator and rudder control forces

(2) Possible interaction of elevator and rudder trimming when tabs are at fairly large deflections

(3) More complicated operating mechanism

(4) Greater loads on tail and fuselage, which would tend to require increased weight

The tests of the isolated vee tail indicated that the simplified theory developed for vee tails was valid for dihedral angles up to about 40°.

The relative merits of the vee tail and conventional tails for spin recovery have not been established, but it appears that the vee tail should be at least as good as the conventional tail assembly in this respect, except possibly in cases in which simultaneous full deflection of both rudder and elevator is required for recovery from the spin.

INTRODUCTION

Early investigations of vee-tail surfaces were reported in 1932 and 1936 (references 1 and 2). The principal advantage claimed for the vee tail was a reduction in drag which, when compared with the total

airplane drag, was fairly small. As the values of total airplane drag coefficient have decreased, however, a given reduction in tail-surface drag coefficient has become more important. In the last few years more attention has therefore been given to vee-tail surfaces and three investigations have been made by the NACA. One of these investigations included both theoretical and experimental results and was reported in reference 3; the other two investigations were wind-tunnel tests of complete models with various tail-surface arrangements.

The present paper extends the theory of reference 3 to include control effectiveness and control forces as well as stability, summarizes the results of the two complete-model investigations, and reports tests of two isolated tail surfaces with various amounts of dihedral. A method for designing vee tails is also given.

COEFFICIENTS AND SYMBOLS

The coefficients and symbols used herein are defined as follows:

C_L	lift coefficient (Z/qS)
C_{D_R}	resultant-drag coefficient (X/qS)
C_Y	lateral-force coefficient (Y/qS)
C_l	rolling-moment coefficient (L/qSb)
C_m	pitching-moment coefficient (M/qSc)
C_n	yawing-moment coefficient (N/qSb)
C_h	hinge-moment coefficient $(H/qb\bar{c}^2)$
T_c	effective thrust coefficient $(T_e/\rho V^2 D^2)$

where

X,Y,Z	forces along axes defined in figure 1
L,M,N	moments about axes defined in figure 1
H	hinge moment of control surface

[redacted]

T_e	effective thrust
q	dynamic pressure $\left(\frac{1}{2}\rho V^2\right)$
S	actual (not projected) area
c	mean geometric chord
$\bar{c}$	root-mean-square chord of control surface behind hinge line
b	actual (not projected) span
V	airspeed
D	propeller diameter
ρ	mass density of air

and

α	angle of attack of thrust line for complete models and of chord line at plane of symmetry for isolated tails measured in plane of symmetry, degrees
ψ	angle of yaw, degrees
β	angle of sideslip, degrees $(-\psi)$
i_t	angle of stabilizer with respect to fuselage center line measured in plane of symmetry, degrees; positive when trailing edge is down
δ	control-surface deflection measured in plane normal to chord plane of tail surface, degrees
l_t	tail length; distance from center of gravity to hinge line of control surface
ϵ	angle of downwash, degrees
σ	angle of sidewash, degrees
$d\epsilon/d\alpha$	rate of change of downwash angle at tail with angle of attack

[redacted]

$d\sigma/d\beta$ rate of change of sidewash angle at tail with angle of sideslip

A aspect ratio (b^2/S)

λ taper ratio; ratio of tip chord to root chord

F stick or pedal force

The symbols used in the development of the theory of vee tails are defined as follows:

C_{L_t} lift coefficient of tail measured in plane of symmetry

α_t angle of attack of tail measured in plane of symmetry, degrees

C_{Y_t} lateral-force coefficient of tail measured normal to plane of symmetry

β_t angle of sideslip of plane of symmetry

δ_e elevator deflection or elerudder deflection when elerudder surfaces are deflected upward or downward together, degrees

δ_r rudder deflection or elerudder deflection when elerudder surfaces are deflected equal and opposite amounts on the two sides, degrees

δ_{er} deflection of single elerudder surface, degrees; subscripts R and L denote right and left elerudder surfaces, respectively

Γ dihedral angle of tail surface measured from XY-plane of vee tail to each tail panel, degrees

C_{L_N} tail lift coefficient measured in plane normal to chord plane of each tail panel

C_{L_N}' sum of changes in tail lift coefficient normal to each tail panel when tail is yawed; equal and opposite span load distributions overlap so that $C_{L_N}' = KC_{L_N}$, where values for K are presented in figure 2

[redacted]

K ratio of sum of lifts obtained by equal and opposite changes in angle of attack of two semispans of tail to lift obtained by an equal change in angle of attack for complete tail (see fig. 2)

k constant of proportionality

α_N angle of attack measured in plane normal to chord plane of each tail panel, degrees

$C_{L_{\alpha_N}}$ slope of tail lift curve in pitch measured in plane normal to chord plane of each tail panel $\left(\frac{\partial C_{L_N}}{\partial \alpha_N}\right)$

$C_{L_{\alpha_N}}'$ slope of vee-tail lift curve when lift and angles of attack are measured in planes normal to chord planes of two tail panels while angle of attack of tail α_t is held constant and tail is sideslipped $\left(\frac{\partial C_{L_N}'}{\partial \alpha_N}\right)$

$C_{Y_{\beta_t}}$ slope of tail lateral-force curve measured normal to plane of symmetry $\left(\frac{\partial C_{Y_t}}{\partial \beta_t}\right)$

τ control-effectiveness parameter $\left(\frac{\partial C_{L_N}}{\partial \delta} \Big/ \frac{\partial C_{L_N}}{\partial \alpha_N}\right)$

Subscripts:

w wing

t tail

h horizontal tail

v vertical tail

vee vee tail

e elevator

r rudder

[redacted]

er elerudder

f flap

$\beta, \psi, \delta, \alpha$ denote partial derivatives of coefficients with respect to angle of sideslip, angle of yaw, control-surface deflection, and angle of attack, respectively; for example,

$$C_{Y_\beta} = \frac{\partial C_Y}{\partial \beta}$$

SIMPLIFIED THEORY OF VEE TAIL

Basic Assumptions

As indicated in reference 3, an isolated vee tail may be considered a wing having a large amount of dihedral. The basic assumptions usually made for a wing with dihedral are used to derive fairly simple expressions for the stability, control, and control-force parameters for vee tails. The span load distributions computed by use of lifting-line theory for wings with no dihedral and no sweepback are assumed to be valid for wings with dihedral and are assumed to be unaffected by interference at the point where the dihedral changes. The assumption is also made that, when the effective angles of attack of the two panels of a wing with dihedral are changed equal and opposite amounts by sideslipping, the changes in lift coefficient normal to each panel are equal and opposite in sign and are equal in magnitude to the changes resulting from equal and opposite changes in angle of attack of the two panels of a wing with zero dihedral. The assumptions of course become less valid as the dihedral increases.

In order to simplify the analysis further, the longitudinal and directional characteristics are considered independently and the lift and hinge-moment characteristics are assumed to be linear in spite of the large control-surface deflections that are required with vee tails when full elevator and rudder control are applied simultaneously. Considering the longitudinal and directional characteristics independently and not accounting for the nonlinearity in the various coefficient curves results in idealized solutions that must

[redacted]

be modified in practical applications. The degree of modification will of course depend on the characteristics of the control surfaces and airplane under consideration. The solutions derived herein are presented only to indicate the general approach to the problem and to present some idea of the comparative characteristics of vee and conventional tails in the idealized case.

With these assumptions as a basis, the following relationships were developed and are illustrated in figure 3:

(1) For small angles of attack, the angle of attack measured in the plane normal to each panel of a vee tail is equal to the angle of attack measured in the plane of symmetry multiplied by the cosine of the tail dihedral angle (fig. 3(a)); thus

$$\alpha_N = \alpha_t \cos \Gamma \tag{1}$$

(2) For small angles of sideslip, the changes in angle of attack measured in the planes normal to each panel of the vee tail are equal and opposite in sign and are equal to the angle of sideslip multiplied by the sine of the tail dihedral angle (fig. 3(b)); thus

$$\alpha_N = \beta_t \sin \Gamma \tag{2}$$

(3) The lift coefficient measured in the plane of symmetry is equal to the lift coefficient measured in the plane normal to each panel of the vee tail multiplied by the cosine of the tail dihedral angle (fig. 3(c)); thus

$$C_{L_t} = C_{L_N} \cos \Gamma \tag{3}$$

(4) When the vee tail is sideslipped, the changes in lift coefficient normal to each panel are equal and opposite in sign and the lateral-force coefficient of

the vee tail is equal to the sum of the changes in lift coefficient normal to each panel of the vee tail multiplied by the sine of the tail dihedral angle (fig. 3(d)); thus

$$C_{Y_t} = C_{L_N}' \sin \Gamma \tag{4}$$

Stability and Control Parameters

The stability and control parameters for an isolated vee tail correspond to the lift and lateral-force parameters for a wing with dihedral and can be developed from equations (1) to (4) as follows:

(1) Longitudinal stability as measured by $C_{L_{\alpha_t}}$:

$$C_{L_{\alpha_t}} = \frac{\partial C_{L_t}}{\partial \alpha_t} = \frac{\partial \left(C_{L_N} \cos \Gamma \right)}{\partial \frac{\alpha_N}{\cos \Gamma}}$$

$$= C_{L_{\alpha_N}} \cos^2 \Gamma \tag{5}$$

(2) Longitudinal control as measured by $C_{L_{\delta_e}}$:

$$C_{L_{\delta_e}} = \frac{\partial C_{L_t}}{\partial \delta_e} = \frac{\partial \left(C_{L_N} \cos \Gamma \right)_T}{\partial \alpha_N}$$

$$= C_{L_{\alpha_N}}{}_T \cos \Gamma \tag{6}$$

(3) Directional stability as measured by $C_{Y_{\beta_t}}$:

$$C_{Y_{\beta_t}} = \frac{\partial C_{Y_t}}{\partial \beta_t} = - \frac{\partial \left(C_{L_N}' \sin \Gamma \right)}{\partial \frac{\alpha_N}{\sin \Gamma}} = -C_{L_{\alpha_N}}' \sin^2 \Gamma$$

$$= -KC_{L_{\alpha_N}} \sin^2 \Gamma \tag{7}$$

[redacted]

(4) Directional control as measured by $C_{Y_{\delta_r}}$:

$$C_{Y_{\delta_r}} = \frac{\partial C_{Y_t}}{\partial \delta_r} = \frac{\partial (C_{L_N}' \sin \Gamma)}{\partial \alpha_N} \tau = C_{L_{\alpha_N}}' \tau \sin \Gamma$$

$$= K C_{L_{\alpha_N}} \tau \sin \Gamma \qquad (8)$$

The relation between the stability parameters $C_{L_{\alpha_t}}$ and $C_{Y_{\beta_t}}$ for vee tails may be obtained as

$$\frac{C_{Y_{\beta_t}}}{C_{L_{\alpha_t}}} = \frac{-K C_{L_{\alpha_N}} \sin^2 \Gamma}{C_{L_{\alpha_N}} \cos^2 \Gamma}$$

$$= -K \tan^2 \Gamma \qquad (9)$$

The relation between the control parameters $C_{L_{\delta_e}}$ and $C_{Y_{\delta_r}}$ may be obtained similarly as

$$\frac{C_{Y_{\delta_r}}}{C_{L_{\delta_e}}} = \frac{K C_{L_{\alpha_N}} \tau \sin \Gamma}{C_{L_{\alpha_N}} \tau \cos \Gamma}$$

$$= K \tan \Gamma \qquad (10)$$

Values of K $\left(\text{or } \frac{C_{L_{\alpha_N}}'}{C_{L_{\alpha_N}}} \right)$ for various aspect ratios and taper ratios are presented in figure 2. The values were obtained from extrapolation of values of K determined from figure 2 of reference 4 by graphically integrating the complete load curves for $1.00\frac{b}{2}$, integrating the right-hand half of the load curve minus the left-hand half, and taking the ratio of the two values.

Comparison of Stability and Control of Vee and Conventional Tails

The relation between the total areas of an isolated vee tail and an isolated conventional tail assembly that provide equal stability can be obtained as follows:

For equal values of $(C_{m_\alpha})_t$ for the vee tail and the conventional horizontal tail,

$$S_h C_{L_{\alpha_{t_h}}} = S_{vee} C_{L_{\alpha_{t_{vee}}}}$$

$$= S_{vee} C_{L_{\alpha_N}} \cos^2\Gamma \qquad (11)$$

For equal values of $(C_{n_\beta})_t$ for the vee tail and the conventional vertical tail,

$$S_v C_{Y_{\beta_{t_v}}} = S_{vee} C_{Y_{\beta_{t_{vee}}}}$$

$$= S_{vee} K C_{L_{\alpha_N}} \sin^2\Gamma \qquad (12)$$

If the horizontal tail and the vee tail are assumed to have the same aspect ratio,

$$C_{L_{\alpha_{t_h}}} = C_{L_{\alpha_N}}$$

If the effective aspect ratio of the vee tail, which for lateral-force computations is lower than its geometric aspect ratio because of the factor K, is assumed to be equal to the effective aspect ratio of the vertical tail, which is higher than its geometric aspect ratio because of the end-plate effect of the horizontal tail,

[redacted]

$$C_{Y_{\beta_{t_v}}} = KC_{L_{\alpha_N}}$$

The assumption of equal lift-curve slopes simplifies equations (11) and (12) to

$$S_h = S_{vee} \cos^2\Gamma \tag{13}$$

and

$$S_v = S_{vee} \sin^2\Gamma \tag{14}$$

When equations (13) and (14) are combined,

$$S_h + S_v = S_{vee}(\cos^2\Gamma + \sin^2\Gamma) \tag{15}$$

But

$$\cos^2\Gamma + \sin^2\Gamma = 1$$

so that

$$S_h + S_v = S_{vee} \tag{16}$$

An isolated vee-tail surface producing stability parameters equal to those produced by an isolated conventional tail assembly (and having equal effective aspect ratios) must therefore have an area equal to that of the conventional tail assembly.

If the areas of a vee tail and a conventional tail assembly are assumed to be made equal to give equal stability and if equal values of the control-effectiveness factor τ are assumed, the control parameters for the isolated vee tail are greater than for the isolated conventional tail assembly by the following ratios:

$$\frac{C_{m_{\delta_{e_{vee}}}}}{C_{m_{\delta_{e_h}}}} = \frac{1}{\cos\Gamma} \tag{17a}$$

[redacted]

and

$$\frac{C_{n_{\delta_{r_{vee}}}}}{C_{n_{\delta_{r_v}}}} = \frac{1}{\sin \Gamma} \tag{17b}$$

For equal total areas and equal values of $(C_{m_\alpha})_t$ and $C_{m_{\delta_e}}$ for the vee tail and the conventional tail assembly, the required control-effectiveness factor τ is smaller for the vee tail than for the conventional tails because

$$\frac{\tau_{vee}}{\tau_h} = \cos \Gamma \tag{18a}$$

and

$$\frac{\tau_{vee}}{\tau_v} = \sin \Gamma \tag{18b}$$

The foregoing analysis is based on the assumptions that the control characteristics are linear over the entire range of control deflections and that a vee tail having values of the control parameters $C_{m_{\delta_e}}$ and $C_{n_{\delta_r}}$ equal to those for the conventional tail could produce the same maximum control as the conventional control surfaces by having a maximum elerudder deflection equal to the sum of the maximum rudder and elevator deflections with the conventional tails. In many practical cases, however, these assumptions will not be valid because control effectiveness per unit deflection decreases at large deflections, and the vee tail will consequently compare less favorably with the conventional tails than equations (18) indicate. In fact, if the conventional elevator and rudder are already using the maximum practicable control-deflection range, the vee-tail elerudder deflection will also be restricted to this range and the vee tail will consequently require a much greater control-effectiveness factor τ (and therefore a control surface of larger chord ratio) than the conventional tails.

[redacted]

Comparison of Control-Force Characteristics of Vee and Conventional Tails

A general solution relating the control-force characteristics of vee-tail and conventional tail surfaces cannot easily be obtained since, in the design of equivalent surfaces of the two types, equal values of the longitudinal or directional stability and control parameters may be obtained by several variations of the geometrical relationship between the two types of tail. Usually it will be impossible to obtain equal values of all the parameters $(C_{m_\alpha})_t$, $C_{m_{\delta_e}}$, $(C_{n_\beta})_t$, and $C_{n_{\delta_r}}$ for the two types of tail. By considering the longitudinal and directional characteristics independently and by making certain simplifying assumptions, however, expressions can be derived that relate the longitudinal or directional control forces for vee tails and conventional tails.

Elevator forces.- The elevator control forces of a vee tail and a conventional horizontal tail can be related by neglecting the directional stability and control characteristics and by assuming equal values of $C_{m_{\alpha_t}}$, $C_{m_{\delta_e}}$, tail length, aspect ratio, and gearing of elevator to control stick for the two tails.

For equivalent longitudinal stability and control and with the same aspect ratio of the conventional and vee tails, it has been shown (equations (13) and (18a)) that the area of the vee tail is related to the area of the conventional tail by $\cos^2\Gamma$ and that the control-effectiveness parameters of the two types of tail are related by $\cos\Gamma$. For the horizontal tail and a vee tail having the same aspect ratio, the following expressions may be derived from equation (13):

$$b_{vee} = \frac{b_h}{\cos\Gamma} \qquad (19)$$

and

$$c_{vee} = \frac{c_h}{\cos\Gamma} \qquad (20)$$

[redacted]

Equation (18a) indicates that, for a given value of $C_{m_{\delta_e}}$, the vee tail requires a control surface of smaller chord ratio than the conventional horizontal tail but, since the over-all tail chord is greater, the actual control-surface chord may be greater or less. An analysis of the data of reference 5 indicated that the required control-surface chord ratio is proportional to some power n of the effectiveness. A logarithmic plot of the effectiveness data in figure 1(a) of reference 5 and figure 1(b) of reference 6 indicates that an average value of the exponent n is 1.7 for plain sealed flaps having chord ratios between 0.10 and 0.60. Thus

$$\frac{\overline{c_e}}{c_h} = k\tau_h^n$$

and

$$\frac{\overline{c_{er}}}{c_{vee}} = k\tau_{vee}^n$$

Then

$$\frac{\overline{c_{er}}}{c_{vee}} = \frac{\overline{c_e}}{c_h}\left(\frac{\tau_{vee}}{\tau_h}\right)^n$$

or

$$\frac{\overline{c_{er}}}{\overline{c_e}} = \frac{\frac{c_h}{\cos\Gamma}}{c_h}\left(\frac{\tau_{vee}}{\tau_h}\right)^n = \frac{1}{\cos\Gamma}\left(\frac{\tau_{vee}}{\tau_h}\right)^n$$

Therefore

$$\frac{\overline{c_{er}}}{\overline{c_e}} = \frac{1}{\cos\Gamma}\cos^n\Gamma = \cos^{n-1}\Gamma$$

[redacted]

or

$$\overline{c_{er}} = \overline{c_e} \cos^{n-1}\Gamma \tag{21}$$

The stick force is proportional to some factor multiplied by the product of the hinge-moment coefficient, the control-surface span, and the square of the control-surface chord. Since the factor is the same for equivalent conventional and vee tails,

$$\frac{F_{vee}}{F_h} = \frac{C_{h_{vee}}}{C_{h_h}} \frac{b_{vee}\overline{c_{er}}^2}{b_h\overline{c_e}^2}$$

$$= \frac{C_{h_{vee}}}{C_{h_h}} \frac{\frac{b_h}{\cos\Gamma}}{b_h} \frac{\left(\overline{c_e}\cos^{n-1}\Gamma\right)^2}{\overline{c_e}^2}$$

$$= \frac{1}{\cos\Gamma}\left(\cos^{n-1}\Gamma\right)^2 \frac{C_{h_{vee}}}{C_{h_h}}$$

$$= \cos^{2n-3}\Gamma \frac{C_{h_{vee}}}{C_{h_h}} \tag{22}$$

When $n = 1.7$, equation (22) reduces to

$$\frac{F_{vee}}{F_h} = \cos^{0.4}\Gamma \frac{C_{h_{vee}}}{C_{h_h}} \tag{23a}$$

Since the value of the cosine is less than 1 for all values of the dihedral angle except 0° (for example, $\cos^{0.4}45^\circ = 0.87$), the stick force for a vee tail

should be less than for an equivalent conventional tail if the hinge-moment coefficients are equal. Similarly, if the stick forces are equal, the vee-tail control surfaces generally do not need to be so closely balanced as the conventional surfaces.

Different assumptions in the analysis will naturally lead to different results, some of which will be more favorable to the vee tail and some of which will be more favorable to the conventional tail. The present analysis, however, indicates that some reduction in control force or amount of balance required can be obtained by use of the vee tail.

Rudder forces.- In a similar analysis of rudder forces, it was assumed that the mean chords of the two types of tail are equal and that, for the average case, the resulting increased aspect ratio of the vee tail offsets the end-plate effect of the horizontal tail on the vertical tail and causes $C_{L_{\alpha_N}}$' to be equal to $(C_{Y_\beta})_{t_v}$. The result of this analysis was

$$\frac{F_{vee}}{F_v} = \sin^{1.4}\Gamma \frac{C_{h_{vee}}}{C_{h_v}} \tag{23b}$$

which again indicates that the vee tail can have lower control forces or can require less balance for the same forces than the conventional tail.

Limitations of Present Analysis

In the previously developed formulas relating the control forces of vee and conventional tails, the elevator and rudder forces are considered separately and no account is taken of the fact that the lift and hinge-moment curves of actual control surfaces are linear functions of angle of attack and control-surface deflection for only small ranges of these angles. In practical applications of vee tails, the simultaneous use of full rudder and full elevator control will usually place one of the surfaces at a deflection outside the linear range

[redacted]

of lift and hinge-moment characteristics. This condition may be avoided by using control surfaces of larger chord ratio and smaller deflections. The use of control surfaces of larger chord ratio tends to counteract the decrease in control forces previously shown possible but the smaller deflections required make possible the use of a more favorable control-stick gearing, which might result in a net decrease in control force. The final result will of course depend on the amount of elevator and rudder control required in the specific case and on the degree of linearity of the various characteristics of the particular control surfaces being considered. In many cases these practical aspects of the application not only will cancel the gain in control force shown possible by use of the vee tail but also may even increase the control force.

The preceding analysis, however, indicates that, since in the idealized case the vee tail provides a reduction in control force or balance, the choice of a tail for any given airplane can be made only after a thorough analysis of the requirements of each application.

DESIGN METHODS FOR VEE TAILS

Design Formulas

The following formulas for the vee-tail stability and control parameters were derived by modifying equations (5) to (8) for the isolated vee tail to apply to a vee tail installed on an airplane:

$$(C_{m_\alpha})_t = -\frac{q_t}{q}\left(1 - \frac{\partial\epsilon}{\partial\alpha}\right)\frac{l_t}{c_w} C_{L_{\alpha_N}} \frac{S_{vee}}{S_w} \cos^2\Gamma \qquad (24)$$

$$(C_{n_\beta})_t = \frac{q_t}{q}\left(1 + \frac{\partial\sigma}{\partial\beta}\right)\frac{l_t}{b_w} C_{L_{\alpha_N}} \frac{S_{vee}}{S_w} \sin^2\Gamma$$

$$= \frac{q_t}{q}\left(1 + \frac{\partial\sigma}{\partial\beta}\right)\frac{l_t}{b_w} KC_{L_{\alpha_N}} \frac{S_{vee}}{S_w} \sin^2\Gamma \qquad (25)$$

[redacted]

$$C_{m_{\delta_e}} = -\frac{q_t}{q}\tau\frac{l_t}{c_w}C_{L_{\alpha_N}}\frac{S_{vee}}{S_w}\cos\Gamma \qquad (26)$$

$$C_{n_{\delta_r}} = -\frac{q_t}{q}\tau\frac{l_t}{b_w}C_{L_{\alpha_N}}\frac{S_{vee}}{S_w}\sin\Gamma$$

$$= -\frac{q_t}{q}\tau\frac{l_t}{b_w}KC_{L_{\alpha_N}}\frac{S_{vee}}{S_w}\sin\Gamma \qquad (27)$$

When equations (24) and (25) are combined, the expression for finding the dihedral required for the vee tail is

$$\tan^2\Gamma = -\frac{\frac{b_w}{c_w}\left(1 - \frac{\partial\epsilon}{\partial\sigma}\right)(C_{n_\beta})_t}{K\left(1 + \frac{\partial\sigma}{\partial\beta}\right)(C_{m_\alpha})_t} \qquad (28)$$

Equations (24) and (25) may be rearranged to give the following expressions for the area required for the vee tail:

$$\frac{S_{vee}}{S_w} = -\frac{(C_{m_\alpha})_t}{\frac{q_t}{q}\frac{l_t}{c_w}C_{L_{\alpha_N}}\left(1 - \frac{\partial\epsilon}{\partial\alpha}\right)\cos^2\Gamma} \qquad (29)$$

and

$$\frac{S_{vee}}{S_w} = \frac{(C_{n_\beta})_t}{\frac{q_t}{q}\frac{l_t}{b_w}KC_{L_{\alpha_N}}\left(1 + \frac{\partial\sigma}{\partial\beta}\right)\sin^2\Gamma} \qquad (30)$$

Equations (26) and (27) may be rearranged to give the following expressions for the control-effectiveness factor τ required for the vee tail:

[redacted]

$$\tau = -\frac{C_{m_{\delta_e}}}{\frac{q_t}{q}\frac{l_t}{c_w} C_{L_{\alpha_N}} \frac{S_{vee}}{S_w} \cos \Gamma} \tag{31}$$

and

$$\tau = -\frac{C_{n_{\delta_r}}}{\frac{q_t}{q}\frac{l_t}{b_w} KC_{L_{\alpha_N}} \frac{S_{vee}}{S_w} \sin \Gamma} \tag{32}$$

Design Procedure

The steps in designing a vee tail to produce desired values of the stability and control parameters may be outlined as follows:

(1) Decide on required values of $(C_{m_\alpha})_t$, $(C_{n_\beta})_t$, $C_{m_{\delta_e}}$, and $C_{n_{\delta_r}}$. The vee tail probably should be designed to produce higher values of $C_{m_{\delta_e}}$ and $C_{n_{\delta_r}}$ than the conventional tails in order that the elerudder deflections can be kept in the linear range of control effectiveness against deflection. This point is discussed more fully in the section entitled "General Remarks."

(2) Determine values of K from figure 2 of the present paper and values of $C_{L_{\alpha_N}}$ from figure 3 of reference 7.

(3) Estimate values of $\partial\sigma/\partial\beta$ and $\partial\epsilon/\partial\alpha$ for an average vee-tail arrangement. Assume $\Gamma = 35^\circ$, $A_t = 4.5$, and $\frac{S_{vee}}{S_w} = 0.25$. References 7 to 9 will be helpful in designing for the power-off and windmilling conditions.

(4) Determine Γ from equation (28).

[redacted]

(5) Determine S_{vee} from equation (29) or (30).

(6) Determine τ from equations (31) and (32).

(7) Substitute the larger of the values of τ obtained from step (6) in equations (26) and (27) to determine final values of $C_{m_{\delta_e}}$ and $C_{n_{\delta_r}}$. One of these two values probably will be larger than necessary since the two values of τ determined from equations (31) and (32) will usually not be identical.

(8) Use the value of τ from step (7) with figure 1(a) of reference 5 to determine the required value of $\overline{c_{er}}/c_{voe}$.

TEST DATA

Presentation of Data

In order to provide a check of the preceding development of a simplified theory for vee tails, force tests of two isolated tail surfaces (tail surfaces A and B of fig. 4) with various amounts of dihedral were made in the Langley free-flight tunnel. A test was also made of tail surface B with one tail panel removed to simulate an isolated vertical tail or the condition approached by a vee tail with a dihedral angle of 90°. These data are presented in figures 5 to 9. A complete list of figures is presented in table I.

Some of the data obtained in force tests of a complete airplane model (figs. 10 and 11) in the Langley 7- by 10-foot tunnel and in force and flight tests of a complete model of a fighter airplane (fig. 12) in the Langley free-flight tunnel are presented in figures 13 to 20.

The results of the tests are presented in standard NACA coefficients of forces and moments. The data are referred to a system of axes in which the Z-axis is in the plane of symmetry and perpendicular to the relative wind, the X-axis is in the plane of symmetry and perpendicular to the Z-axis, and the Y-axis is perpendicular to the plane of symmetry. (See fig. 1.)

[redacted]

Test Conditions

The force tests of the two isolated tail surfaces A and B were made in the Langley free-flight tunnel at a dynamic pressure of 4.09 pounds per square foot, which corresponds to an airspeed of about 40 miles per hour. The test Reynolds numbers were about 199,000 for tail surface A based on the tail mean geometric chord of 6.23 inches and 256,000 for tail surface B based on the tail mean geometric chord of 8.01 inches. The effective Reynolds numbers, based on a turbulence factor of 1.6 for the Langley free-flight tunnel, were about 319,000 for tail surface A and 410,000 for tail surface B.

The complete-model tests in the Langley 7- by 10-foot tunnel were made at a dynamic pressure of 16.37 pounds per square foot, which corresponds to an airspeed of about 80 miles per hour. The test Reynolds number was about 733,000 based on the wing mean geometric chord of 12.04 inches. Because of the turbulence factor of 1.6 for the tunnel, the effective Reynolds number was about 1,173,000.

The force tests of the fighter-airplane model were made in the Langley free-flight tunnel at a dynamic pressure of 1.9 pounds per square foot, which corresponds to an airspeed of about 27 miles per hour. The test Reynolds number was about 166,000 based on the wing mean geometric chord of 7.76 inches. The effective Reynolds number, based on the turbulence factor of about 1.6 for the tunnel, was about 266,000.

All coefficients for the data obtained in the complete-model tests are based on the area, span, and mean chord of the model wing. All coefficients for the isolated-tail data are based on the area, span, and mean chord of the complete tail surface. The coefficients for the single panel of tail surface B are also based on the area, span, and chord of the complete tail surface in order that the data may be considered to apply to a vee tail with a dihedral angle of 30°.

Corrections

None of the data have been corrected for the tares caused by the model support strut. Jet-boundary corrections have been applied to the angles of attack, the

[redacted]

drag coefficients, and the tail-on pitching-moment coefficients from tests in the Langley 7- by 10-foot tunnel. These corrections were computed as follows:

$$\Delta\alpha = 57.3(\delta_w + 0.017c)\frac{S}{C}C_L \qquad \text{(deg)}$$

$$\Delta C_{D_R} = \delta_w\frac{S}{C}C_L^2$$

$$\Delta C_m = -57.3\left(\frac{\delta_T}{\sqrt{q_t/q}} - \delta_w\right)\frac{S}{C}\frac{\partial C_m}{\partial i_t}C_L$$

where

δ_w jet-boundary correction factor at wing (0.119)

δ_T total jet-boundary correction at tail (0.201 - 0.00083α)

S model wing area (8.025 ft)

c model mean geometric chord (1.003 ft)

C tunnel cross-sectional area (69.59 sq ft)

$\frac{\partial C_m}{\partial i_t}$ change in pitching-moment coefficient per degree change in stabilizer setting as determined in present tests

q_t/q ratio of effective dynamic pressure over horizontal tail to free-stream dynamic pressure (assumed to equal 1.0 for this model)

All corrections were added to the test data. No corrections have been applied to the force-test data obtained in the Langley free-flight tunnel, because the tunnel cross-sectional area C is large in comparison with the wing area of the models S and the corrections are negligible.

[redacted]

Tests of Isolated Vee Tails

Results of tests of isolated vee tails are shown in figures 5 and 6, in which lift and lateral-force parameters are plotted against dihedral angle for tail surfaces A and B. The results are generalized as variations of lift and lateral-force parameter ratios with dihedral angle as shown in figure 7. The data in figures 5 to 7 indicate that the simplified theory developed in preceding sections of the present paper is adequate. The principal discrepancies between the theoretical and experimental results occur for the lateral-force-curve slopes at dihedral angles greater than 40°. Such a result is to be expected since, as the dihedral angle approaches 90°, the two panels gradually approach the condition of one panel of one-half the area and aspect ratio. This condition is illustrated in figures 6 and 7 by the test point at $\Gamma = 90^\circ$ for one panel of tail surface B.

The data presented in figures 8 and 9 show that the angles at which the lift and lateral-force curves for the vee tail depart from linearity are considerably larger than the angles at which the curves for the normal tail depart from linearity. This result is to be expected, because for vee tails the section angle of attack (or angle of sideslip) is smaller than the angle measured in (or normal to) the plane of symmetry by the cosine (or sine) of the dihedral angle.

The experimental data of figures 8 and 9 give results similar to those obtained in the analysis, which indicated that a vee-tail surface producing stability parameters equal to those produced by a conventional tail assembly would have an area equal to the area of the conventional tail assembly. This result can be illustrated by the slopes of the curves as follows:

Slope	Conventional tail	40° vee tail
C_{L_α}	0.061	0.040 (from fig. 8)
C_{Y_β}	-.024	-.016 (from fig. 9)

where all coefficients are based on the area of two tail panels. These values of C_{L_α} and C_{Y_β} for the

[redacted]

conventional tails are about 1.5 times as large as the values for the vee tail, but the conventional tail assembly also has 1.5 times as much area as the vee tail because it is made up of three panels identical with the two panels of the vee tail. It therefore follows that, if this vee tail is scaled up so that its area is equal to the total area of the conventional tail assembly, the stability parameters produced by the vee tail will be approximately equal to those produced by the horizontal and vertical tails.

The experimental data of figures 8 and 9 indicate that, since C_{Y_β} = 0.048 (based on area of vertical tail) and $KC_{L_{\alpha_N}}$ = 0.67 × 0.061 = 0.041, the effective aspect ratio of the vertical tail was greater than the effective aspect ratio of the vee tail in sideslip, even though the vertical tail was tested in the isolated condition and did not have the beneficial end-plate effect of the horizontal tail. This result is attributed to the fact that the geometric aspect ratio of the vertical tail was relatively higher than usual (one-half that of the vee tail) and to the fact that the effective aspect ratio of the vertical tail was higher than its geometric aspect ratio, possibly because of an end-plate effect of the streamline fairing. In practical cases, the vertical tail and vee tail probably will have approximately the same effective aspect ratio because the vertical tail will usually have an aspect ratio less than one-half that of the vee tail although it will benefit from the end-plate effect of the horizontal tail.

For the isolated tail, no reduction in total area appears to result from the use of a vee tail unless a higher effective aspect ratio is used for the vee-tail surfaces than for the conventional tail surfaces. For the two complete models tested to date, the vee-tail surfaces have had much higher geometric aspect ratios and probably higher effective aspect ratios. For the fighter-airplane model tested in the Langley free-flight tunnel, for example, the values of geometric aspect ratio were 5.1, 3.9, and 1.1 for the vee, horizontal, and vertical tail surfaces, respectively. A higher aspect ratio appears to be the principal factor contributing to the reduction in total tail area found possible for a vee tail and is of course not an inherent characteristic of a vee tail. Part of the reduction,

however, might have been caused by the higher location of the vee tail, which places it in a region of less downwash particularly for high power conditions, or by the shape of the vee tail, which places it away from the wake of the cockpit canopy.

Tests of Complete Models

Data from tests of complete models in the Langley 7- by 10-foot tunnel and in the Langley free-flight tunnel are presented in figures 13 to 20.

Tests in Langley 7- by 10-foot tunnel.- A three-view drawing of the complete model and details of the tail surfaces tested in the Langley 7- by 10-foot tunnel are shown in figures 10 and 11. In these tests the only unusual result to be noted is that the longitudinal stability contributed by the vee tail, which from equation (24) should have been equal to that contributed by the conventional tail, was about 10 percent greater (figs. 13 to 16). The increased effectiveness was probably caused by improved tail-fuselage junctures. Similarly, the vee tail was about 10 percent more effective in yaw than a theoretical comparison of the two tails indicated.

The effects of rudder deflection on the model with the vee tail and with the conventional tail at high and low angles of attack ($\alpha = 0.1^\circ$ and 8.7°) are presented in figure 15. Some asymmetry of the pitching moments due to the vee tail in yaw was noted when the elerudders were deflected differentially as rudders. The asymmetry, particularly at $\alpha = 8.7^\circ$ (fig. 15(b)), occurs because in the positive angle-of-attack range the slope of the curve of lift coefficient against angle of attack is greater when a plain flap is at a large negative deflection than when the same flap is at a positive deflection. Thus, since the effective angle of attack of the vee tail varies with yaw and since the tail was already at a positive angle of attack, the left-hand half of the tail, which had a negative deflection, was operating in a range in which the slope of the lift curve was higher than that for the right-hand half, which had a positive deflection. The change in pitching moment with rudder deflection at zero yaw was a result of simple nonlinearity in the curve of lift against deflection.

[redacted]

The data of figure 15 also show that the ratio of adverse rolling moments to favorable yawing moments produced by rudder deflection is greater for the vee tail than for the conventional vertical tail.

Additional problems involved in simultaneous operation of the controls are the change in elevator stick force when a large rudder deflection carries one surface out of the linear range, and vice versa, and the possible change in trim about one axis when large tab deflections are required for trim about the other axis. The magnitude of all these effects will of course depend on individual airplane characteristics such as the amount of control or trim required, the length of the linear range of control-surface and tab characteristics, and the relative magnitude of a given change in hinge-moment coefficient when translated into stick or pedal force.

The curves for results of tests of the vee tail in general are more regular and are smoother than the curves for results of tests of the conventional tail, particularly at $\alpha = 0.1^\circ$. For $\alpha = 0.1^\circ$, the conventional fin stalls rather abruptly at angles of yaw of $\pm 15^\circ$ and then regains effectiveness whereas the yawing-moment curves for the vee tail form a relatively straight line for values of ψ up to $\pm 40^\circ$. This characteristic results probably because the section angle of attack of the vee tail is a function of the sine of the angle of yaw and thus the vee tail would be expected to stall at greater angles of yaw than the conventional tail. The inherent tendency of the vee tail toward later stalling is also illustrated in figures 8 and 9.

The plot of the lateral-stability and directional-stability derivatives in figure 16 indicates that neither the vee tail nor the conventional tail appreciably affects the variation of these slopes with lift coefficient. One interesting point is that the vee tail contributed about $1\frac{1}{2}^\circ$ more effective dihedral than the conventional tail although the values of C_{n_ψ} and C_{Y_ψ} were approximately equal for the two tails.

Tests in Langley free-flight tunnel.- A three-view drawing of the complete fighter-airplane model tested in the Langley free-flight tunnel is shown in figure 12. Dimensions of the 36° vee tail and the conventional tail

[redacted]

tested on the model are also given in figure 12. The model was tested with vee-tail dihedral angles varying from 32.4° to 45°.

The results of force tests to determine the longitudinal stability characteristics of the model with the conventional tail and the 36° vee tail are shown in figure 17. The data in figure 17 exhibit no unusual characteristics, and the flight-test data presented in figure 18 provide another quantitative indication that the static longitudinal stability characteristics were essentially equal with the vee and conventional tails. The vee-tail arrangement showed less change of trim with power and flap deflection, probably because of its higher location. During the flights of the model, the pilot could detect no differences in the dynamic stability and handling characteristics with the two tails.

A summary of the stability and control characteristics measured in force tests of the various vee-tail arrangements is presented in figure 19. The scatter of the data in figure 19 is caused partly by the slight variations in area, aspect ratio, and percentage of movable area for the different vee tails as well as in dihedral angle. These results indicate fairly good agreement between experimental and theoretical results except for the values of $(C_{n_\beta})_t$ at dihedral angles greater than 36°. Similar results were noted previously for the isolated-tail tests.

The fighter-airplane model was also tested in the Langley free-flight tunnel on a test stand on which it was free to yaw but was restrained in roll and pitch. An indication of the rudder-force-reversal characteristics of the model with conventional and 43° vee tails was obtained with this setup from the trim angles of yaw produced by different fixed rudder deflections. The results of these tests are presented in figure 20. The tests showed that with the vee tail the model would trim only at fairly small angles of yaw even with full rudder deflection. With the conventional tail, however, the model yawed to large angles with left rudder deflections greater than 13° - an indication that rudder-force reversal or rudder lock probably exists for the airplane with the conventional tail. From these data, therefore, rudder lock appears to be less likely to occur with a vee tail than with a conventional vertical tail. The

[redacted]

previously noted facts that the vee tail stalls at a higher angle of sideslip and may require a control surface of smaller chord ratio than the conventional vertical tail also indicate less tendency toward rudder lock with the vee tail.

GENERAL REMARKS

Stability and Control Characteristics

The foregoing analysis of vee-tail theory and test data has indicated that a vee tail can have the following characteristics relative to those of a conventional tail producing the same values of stability and control parameters:

(1) Approximately equal area unless the conventional vertical tail is in a bad canopy wake, unless the usually higher location of the vee tail places it in a region of greatly reduced downwash, or unless the vee tail has a higher effective aspect ratio than the conventional horizontal and vertical tails.

(2) Possible inadequacy of controls and interaction of control forces when simultaneous full deflection of both controls is required. This difficulty is likely to be encountered if the vee tail is designed to give values of $C_{m_{\delta_e}}$ and $C_{n_{\delta_r}}$ equal to those provided by a conventional tail assembly. It is apparent that, if maximum rudder and elevator deflections of 25° or 30° are used with the conventional tails, elerudder deflections of at least 50° or 60° would be required with the vee tail. At such large deflections, the elerudder would be operating in the nonlinear range of control effectiveness against deflection and might possibly be in the range where the control effectiveness per unit deflection either remained constant or decreased with increasing deflection. One method of avoiding this condition is to use a large balanced elerudder surface that produces larger values of $C_{m_{\delta_e}}$ and $C_{n_{\delta_r}}$ than the conventional-tail control surfaces and therefore produces the required pitching or yawing moments with smaller deflections - not over a total of 30° or 40° - with simultaneous full deflection of both rudder and elevator controls.

[redacted]

(3) Possible interaction between longitudinal and directional trimming when tabs are at fairly large deflections.

(4) Less tendency toward rudder lock.

(5) Possible reduction in control forces or in amount of balance required.

(6) More dihedral effect due to tail.

(7) Larger adverse rolling moments with rudder control.

(8) Less change in trim with application of flaps or power because of the usually higher location of the vee tail.

Additional points not previously considered are that the higher location of the vee tail may decrease the ground effect on the elevator control required for take-off and landing and should also make it simpler to keep the tail out of the spray for take-off and landing in flying boats.

Drag Characteristics

The data from tests in the Langley 7- by 10-foot tunnel shown in figure 13 indicate a decrease of 0.0015 in drag coefficient from use of the vee tail; tests of the same model in the Langley two-dimensional low-turbulence pressure tunnel indicated approximately the same drag reduction. For the model tested, a large part of the reduction was probably caused by a decreased fuselage-tail interference with the vee-tail installation. A vee tail, however, has only two fuselage junctures instead of three and some reduction in drag thus is usually obtained.

Compressibility Effects

For high-speed flight because the vee tail can be installed with a better fuselage-tail juncture, the effects of compressibility on tail drag should be reduced. This advantage, however, tends to be canceled

[redacted]

by the fact that, for vee tails, the individual surfaces will probably be operating at higher lift coefficients for trim and will almost certainly be canceled if the tail is so installed on top of the fuselage that a sharp vee is formed at the juncture. The location of the vee-tail arrangement should place the surfaces farther from the wake of the wing and canopy and thereby should tend to reduce the possibilities of tail buffeting or roughness at high speed.

Spin-Recovery Characteristics

Tests in the Langley 20-foot free-spinning tunnel of a model of the same fighter airplane that was tested in the Langley free-flight tunnel indicated that the vee-tail arrangement had slightly better spin characteristics than the conventional tail assembly. The improved spin characteristics might have occurred because, with the vee tail, there was no horizontal surface to blanket the vertical tail. The data presented in reference 2, although inconclusive, indicated approximately the same spin characteristics for the two types of tail.

At present no general conclusions can be drawn concerning the relative merits of the vee tail and conventional tails for spin recovery. Although available test data indicate that the vee tail may have better spin-recovery characteristics than the conventional tail, it is possible that if simultaneous full deflection of both rudder and elevator is required for spin recovery the vee tail might have less desirable spin-recovery characteristics than the conventional tail assembly.

Structural Considerations

Manufacture and maintenance should be simpler for the vee-tail than for conventional surfaces, since no vertical tail surface must be manufactured, stored, or repaired. The mechanism required to operate the control surfaces both as elevators and as rudders, however, is somewhat complicated and naturally tends to offset this advantage.

The vee tail, because of its configuration, must carry loads that do not contribute to the stability and control. This factor will result in higher tail and

fuselage loads in both pitching and yawing maneuvers, and increased structural weight will be required to carry the greater loads.

CONCLUSIONS

The following conclusions were drawn from the results of the analysis of available data on vee-tail surfaces, from an extension of previously presented vee-tail theory, and from general comparisons of various characteristics of vee-tail and conventional tail surfaces:

1. The use of a vee tail will probably provide no reduction in area unless the conventional vertical tail is in a bad canopy wake, unless the usually higher location of the vee tail places it in a region of greatly reduced downwash, or unless the vee tail has a higher effective aspect ratio than the conventional horizontal and vertical tails.

2. A possible reduction in control forces (or in the amount of control balance required) was indicated by the use of a vee tail, provided that large deflections of the control surface do not cause a large decrease in the effectiveness and increase in hinge-moment coefficient per degree deflection of the control surface. If large-chord control surfaces must be used in order to keep the control deflections small, the control forces (or the amount of control balance required) on the vee tail are likely to be equal to or greater than those for the conventional tail assembly.

3. The following advantages can be obtained with a vee tail designed to provide the same values of stability and control parameters as a conventional tail assembly:

(a) Less drag because vee tail has fewer fuselage-tail junctures

(b) Less tendency toward rudder lock

(c) Higher location of tail surfaces, which tends to reduce elevator deflection required for take-off and landing, to keep the tail out of spray in flying-boat

[redacted]

take-off, and to reduce possibilities of tail buffeting from the wing and canopy wakes in high-speed flight

(d) Fewer tail surfaces to manufacture

4. The following disadvantages tend to counteract the advantages of the vee tail:

(a) Possible interaction of elevator and rudder control forces

(b) Possible interaction of elevator and rudder trimming when tabs are at fairly large deflections

(c) More complicated operating mechanism

(d) Greater loads on tail and fuselage, which would tend to require increased weight

5. The simplified theory of the vee tail is valid for dihedral angles up to about 40°. For dihedral angles greater than 40°, measured directional stability and control parameters were less than indicated by theory.

6. The relative merits of the vee tail and conventional tails for spin recovery have not been established but it appears that the vee tail should be at least as good as the conventional tail assembly in this respect, except possibly in cases in which simultaneous full deflection of both rudder and elevator is required for recovery from the spin.

Langley Memorial Aeronautical Laboratory
National Advisory Committee for Aeronautics
Langley Field, Va.

[redacted]

REFERENCES

1. Anon: The Rudlicki Vee Tail. Aircraft Engineering, vol. IV, no. 37, March 1932, pp. 63-64.

2. Stephens, A. V.: The Vee Tail in Spin. Aircraft Engineering, vol. VIII, no. 93, Nov. 1936, p. 302.

3. Greenberg, Harry: Comparison of Vee-Type and Conventional Tail Surfaces in Combination with Fuselage and Wing in the Variable-Density Tunnel. NACA TN No. 815, 1941.

4. Pearson, Henry A., and Jones, Robert T.: Theoretical Stability and Control Characteristics of Wings with Various Amounts of Taper and Twist. NACA Rep. No. 635, 1938.

5. Swanson, Robert S., and Crandall, Stewart M.: Analysis of Available Data on the Effectiveness of Ailerons without Exposed Overhang Balance. NACA ACR No. L4E01, 1944.

6. Ames, Milton B., Jr., and Sears, Richard I.: Determination of Control-Surface Characteristics from NACA Plain-Flap and Tab Data. NACA Rep. No. 721, 1941.

7. Pass, H. R.: Analysis of Wind-Tunnel Data on Directional Stability and Control. NACA TN No. 775, 1940.

8. Recant, Isidore G., and Wallace, Arthur R.: Wind-Tunnel Investigation of the Effect of Vertical Position of the Wing on the Side Flow in the Region of the Vertical Tail. NACA TN No. 804, 1941.

9. Gilruth, R. R., and White, M. D.: Analysis and Prediction of Longitudinal Stability of Airplanes. NACA Rep. No. 711, 1941.

[redacted]

TABLE I.- PRESENTATION OF RESULTS

Model	Subject	Figure
None	Sign convention for forces, moments, and angles	1
None	Values of K for different aspect ratios and taper ratios	2
None	Relation of angles and force coefficients for vee tails	3
Isolated tail surfaces A and B	Two-view drawing	4
Isolated tail surface A	Variation of lift and lateral-force parameters with dihedral angle	5
Isolated tail surface B	Variation of lift and lateral-force parameters with dihedral angle	6
Isolated tail surfaces A and B	Variation of lift and lateral-force parameter ratios with dihedral angle	7
Isolated tail surface B	C_L against α for $\Gamma = 0^\circ$ (horizontal tail) and $\Gamma = 40^\circ$	8
Isolated tail surface B	C_Y against ψ for $\Gamma = 40^\circ$ and $\Gamma = 90^\circ$ (vertical tail)	9
Complete model (Langley 7- by 10-foot tunnel)	Three-view drawing	10
Do----------	Drawing of conventional and vee tails	11

[redacted]

TABLE I.- PRESENTATION OF RESULTS - Concluded

Model	Subject	Figure
Complete fighter-airplane model (Langley free-flight tunnel)	Three-view drawing	12
Complete model (Langley 7- by 10-foot tunnel)	Stabilizer-effectiveness tests	13
Do----------	Elevator-effectiveness tests	14
Do----------	Rudder-effectiveness tests	15
Do----------	C_{Y_ψ}, C_{n_ψ}, and C_{l_ψ} against C_L	16
Complete fighter-airplane model (Langley free-flight tunnel)	Longitudinal-stability force-test data	17
Do----------	Flight-test data (δ_e against V)	18
Do----------	Variation of stability and control parameters with dihedral angle	19
Do----------	Variation of trim yaw angles with rudder deflection	20

[redacted]

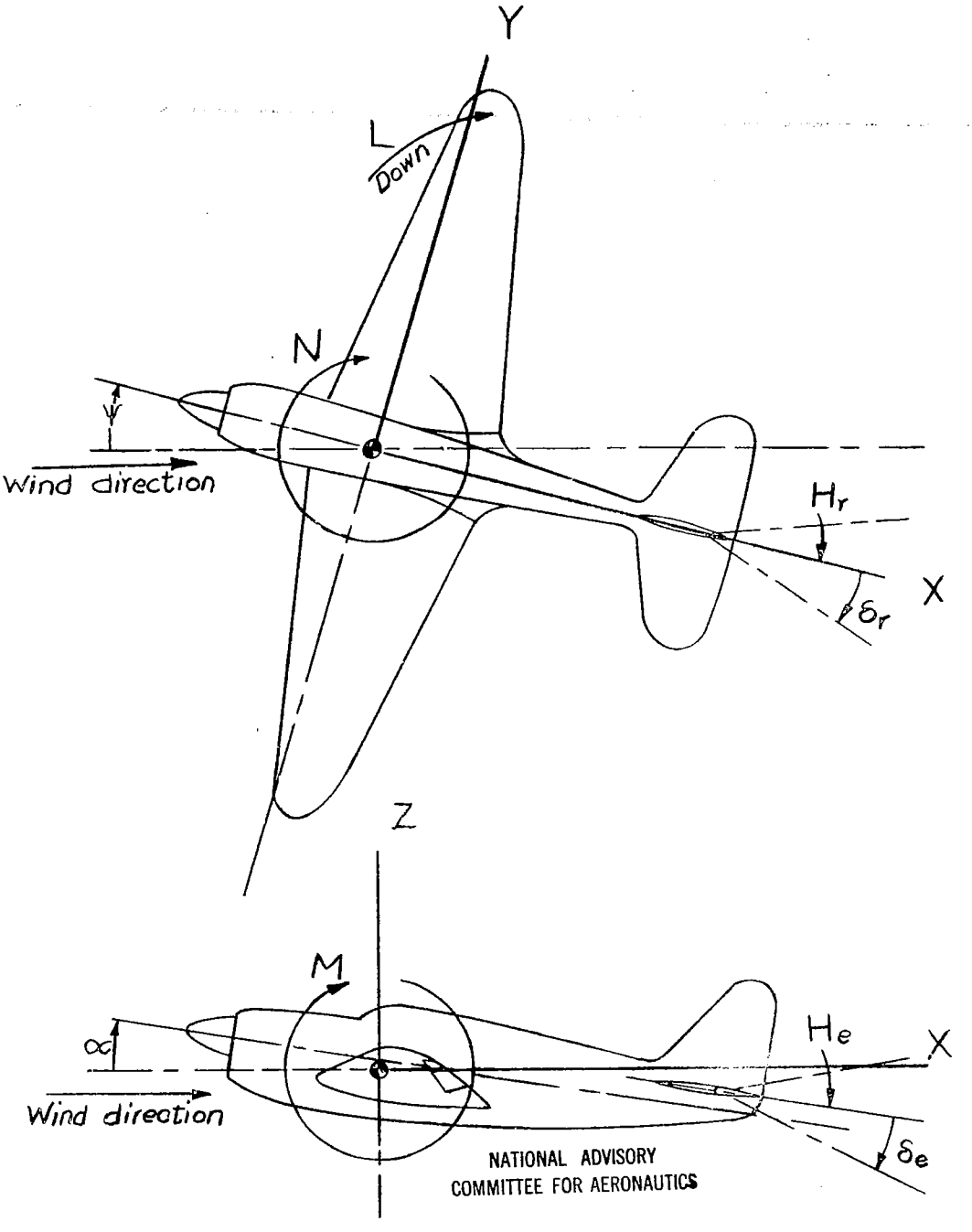

Figure 1.- System of axes and control-surface hinge moments and deflections. Arrows indicate positive directions.

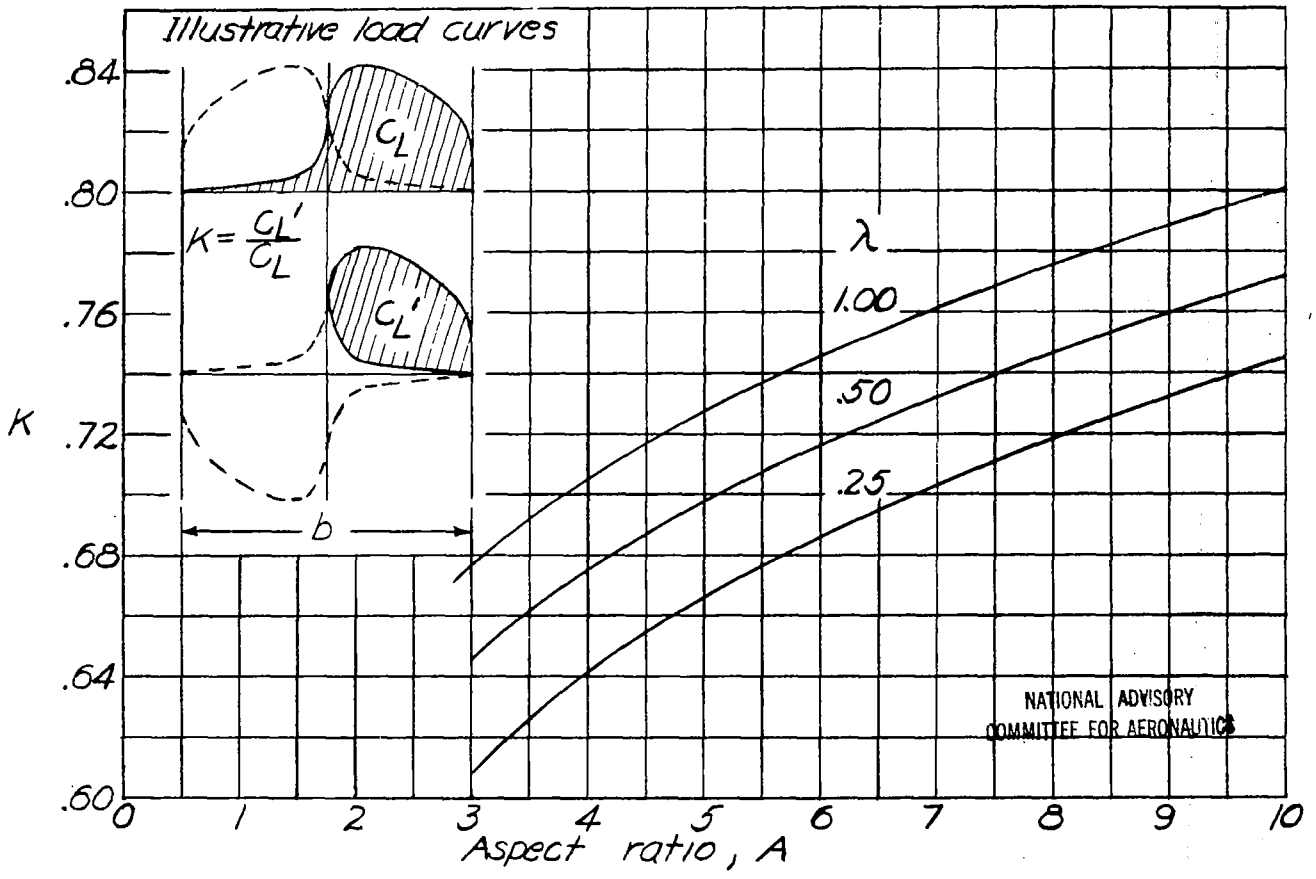

Figure 2.–Values of K for computing slope of lift curve of vee tail in yaw. (Derived from data for round-tipped wings in fig. 2 of reference 4.)

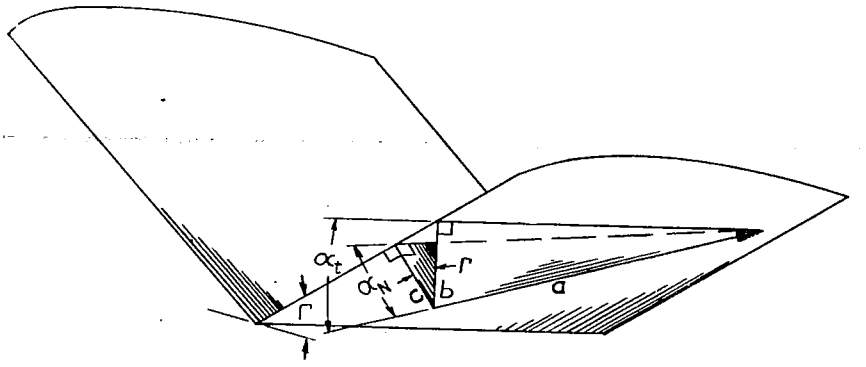

(a) Vee tail in pitch; $\beta_t = 0°$

$\sin \alpha_t = \frac{b}{a}$, or $a = \frac{b}{\sin \alpha_t}$

$\sin \alpha_N = \frac{c}{a}$, or $a = \frac{c}{\sin \alpha_N}$

If α_t and α_N are small

$a = \frac{b}{\alpha_t} = \frac{c}{\alpha_N}$

or $\frac{c}{b} = \frac{\alpha_N}{\alpha_t}$

but $\frac{c}{b} = \cos \Gamma$

$\therefore \frac{\alpha_N}{\alpha_t} = \cos \Gamma$, or $\alpha_N = \alpha_t \cos \Gamma$

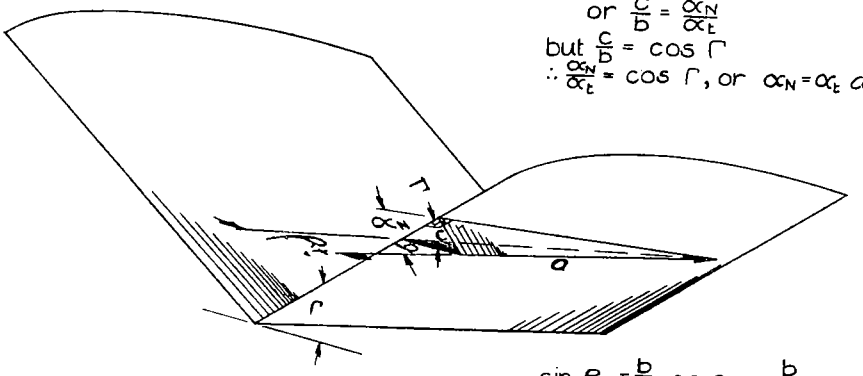

(b) Vee tail in sideslip; $\alpha_t = 0°$

$\sin \beta_t = \frac{b}{a}$, or $a = \frac{b}{\sin \beta_t}$

$\sin \alpha_N = \frac{c}{a}$, or $a = \frac{c}{\sin \alpha_N}$

If β_t and α_N are small

$a = \frac{b}{\beta_t} = \frac{c}{\alpha_N}$

or $\frac{c}{b} = \frac{\alpha_N}{\beta_t}$

but $\frac{c}{b} = \sin \Gamma$

$\therefore \frac{\alpha_N}{\beta_t} = \sin \Gamma$ or $\alpha_N = \beta_t \sin \Gamma$

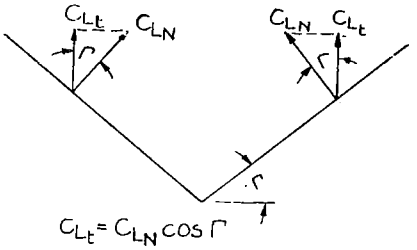

(c) Vee tail in pitch.

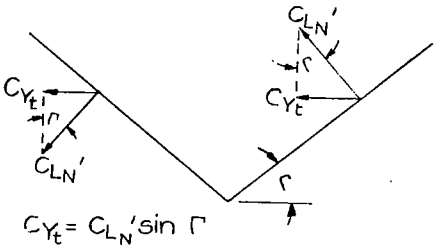

(d) Vee tail in sideslip.

NATIONAL ADVISORY COMMITTEE FOR AERONAUTICS

Figure 3.- Relations of angles and force coefficients for vee tail in pitch and sideslip.

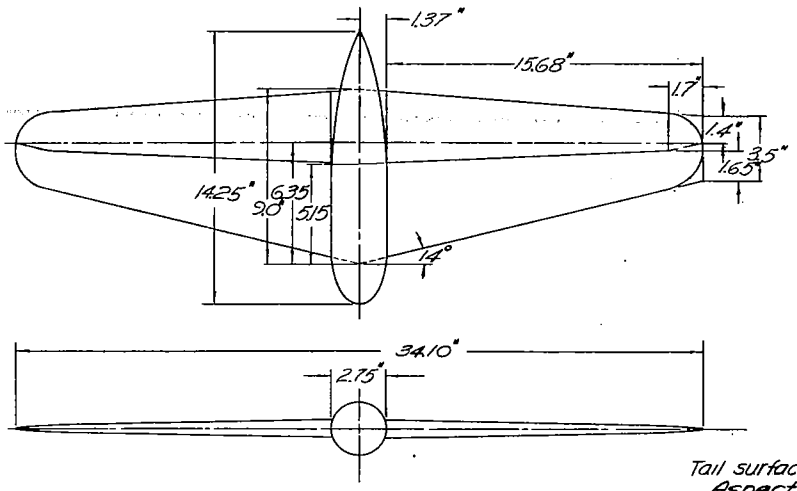

Tail surface A
Aspect ratio = 5.55
Taper ratio = 0.39
Area = 1.48 sq ft
Control-surface area behind hinge line = 0.43 sq ft
Airfoil section = NACA 0012
Dihedral angles = 0°, 19.5°, 38.8°, 51.5°, 59.1°

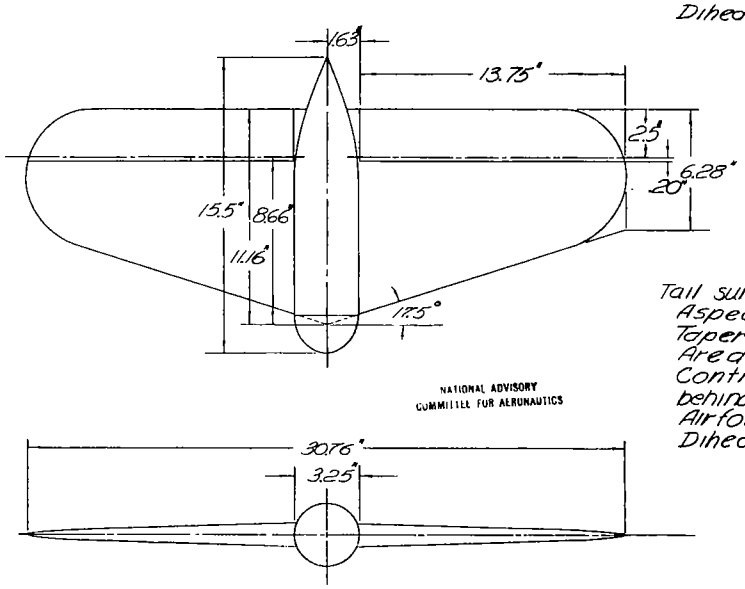

Tail surface B
Aspect ratio = 3.70
Taper ratio = 0.56
Area = 1.78 sq ft
Control-surface area behind hinge line = 0.50 sq ft
Airfoil section = NACA 0009
Dihedral angles = 0°, 30.0°, 39.8°, 50.3°

Figure 4.- Isolated tail surfaces A and B used in force tests in Langley free-flight tunnel to check vee-tail theory.

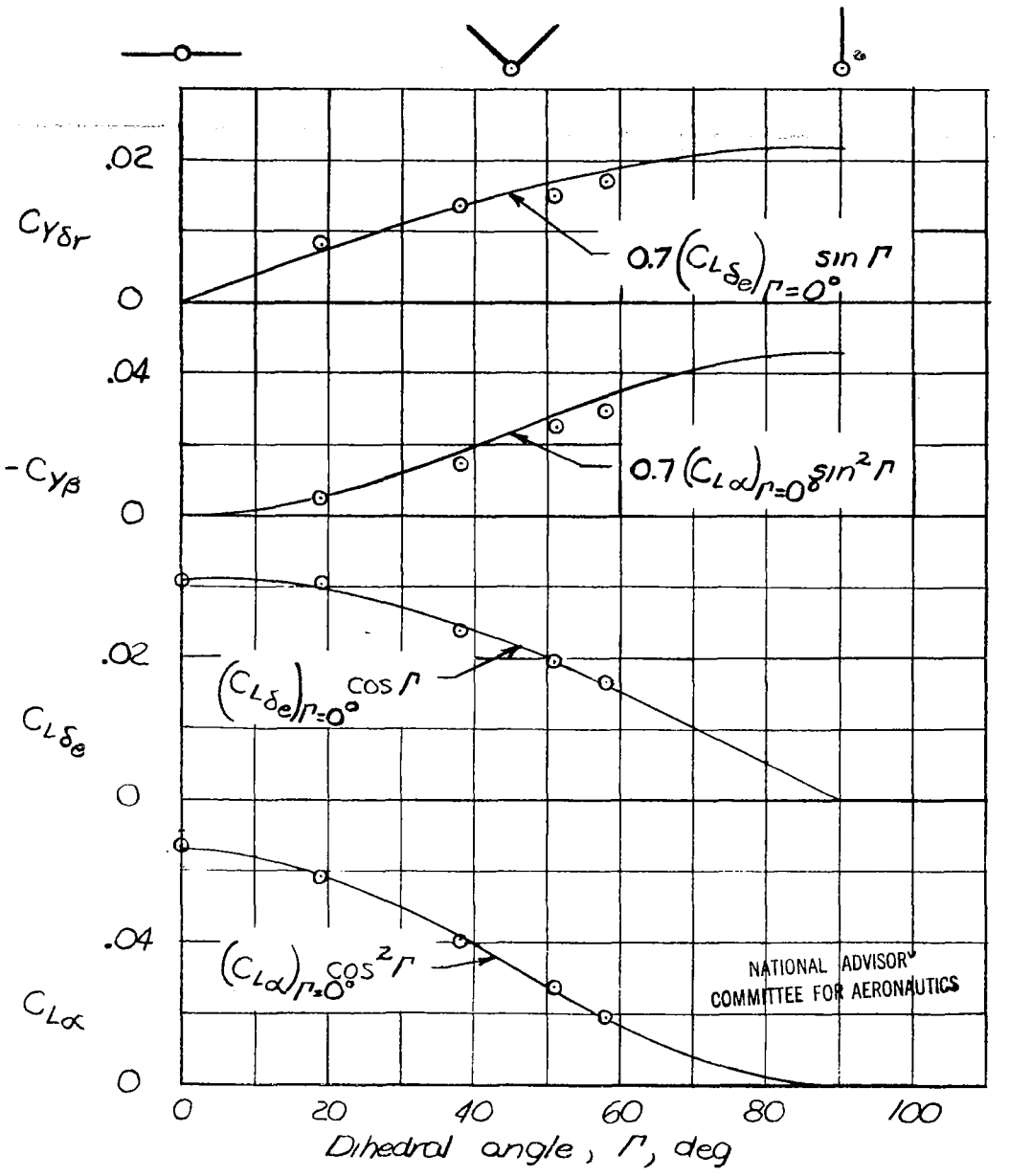

Figure 5.- Variation of lift and lateral-force parameters of isolated tail surface A with tail dihedral angle. $A = 5.55$; $\lambda = 0.39$; $K = 0.70$.

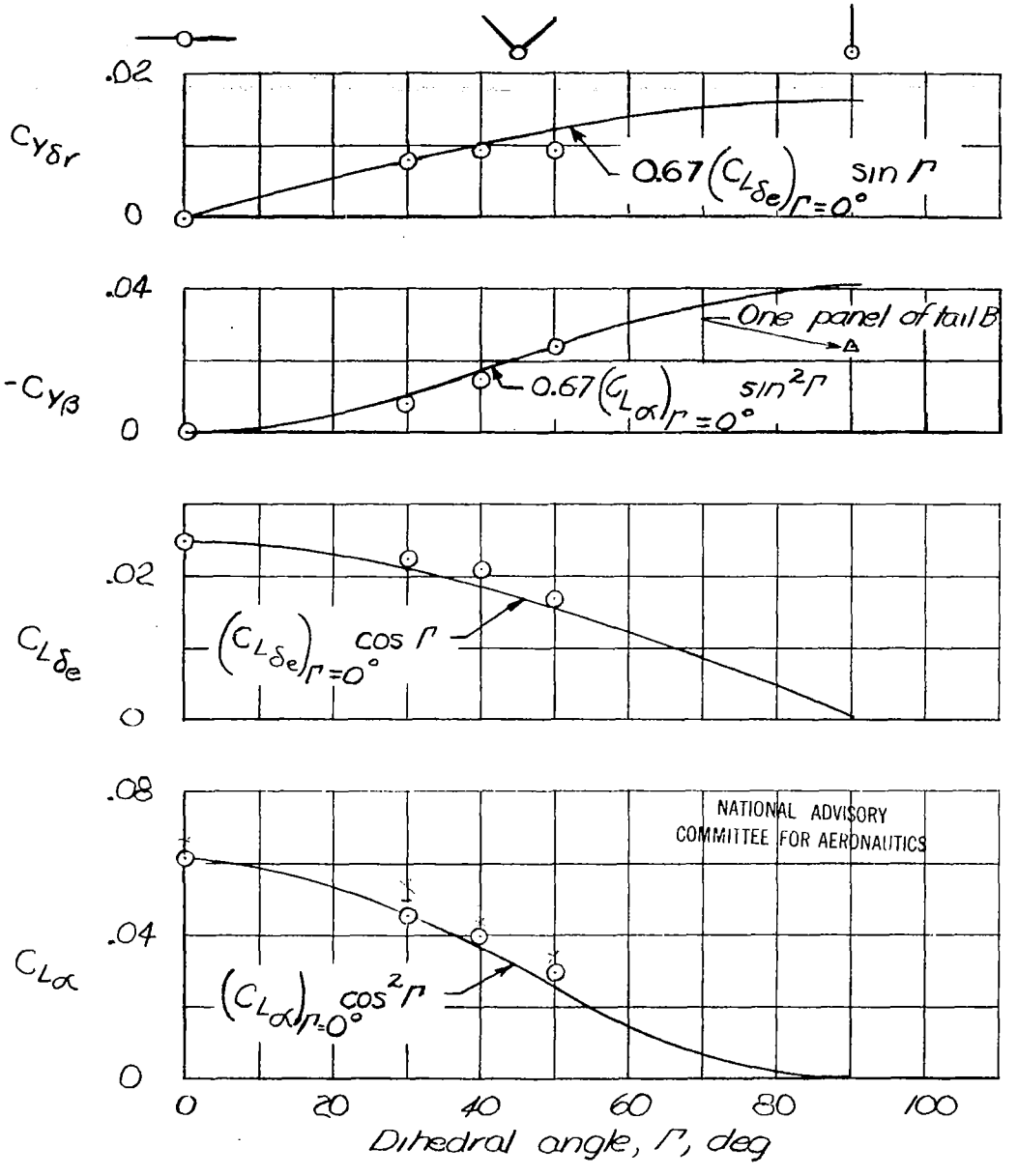

Figure 6.- Variation of lift and lateral-force parameters of isolated tail surface B with tail dihedral angle. $A = 3.70$; $\lambda = 0.56$; $K = 0.67$.

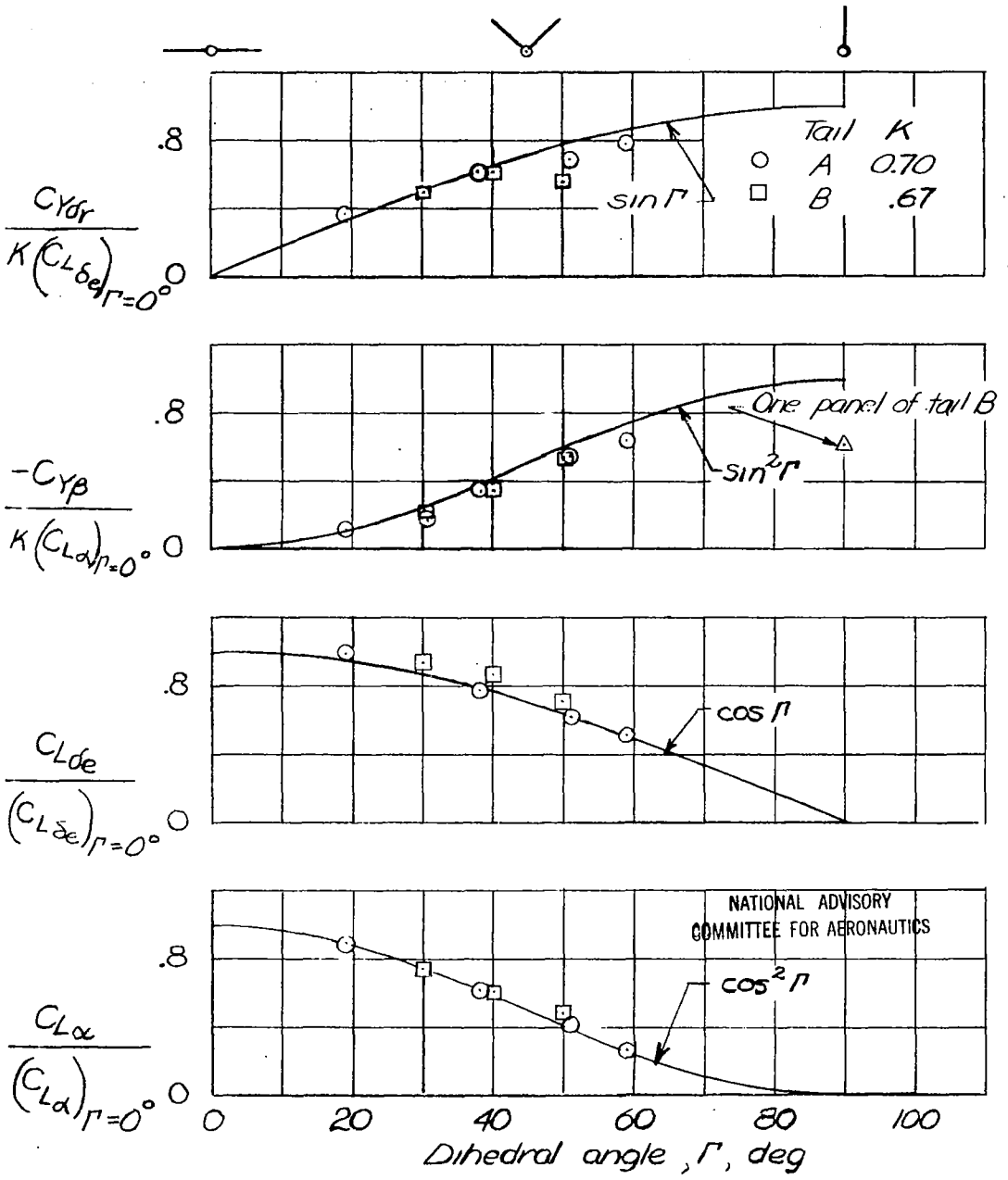

Figure 7.- Variation of lift and lateral-force parameter ratios with vee-tail dihedral angle for isolated tail surfaces A and B.

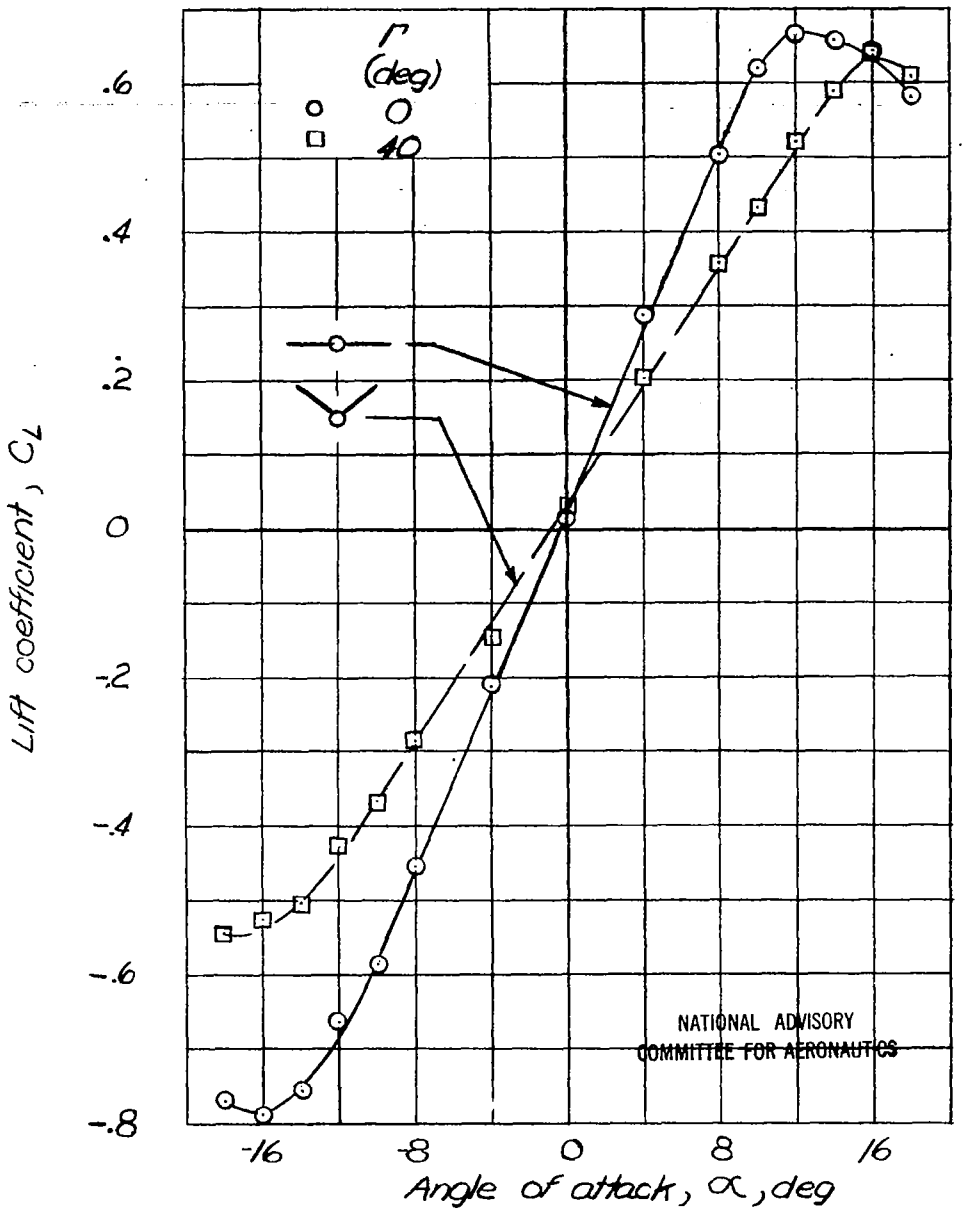

Figure 8.- Variation of lift coefficient with angle of attack for isolated horizontal tail and 40° vee tail. Tail surface B; A = 3.70; λ = 0.56.

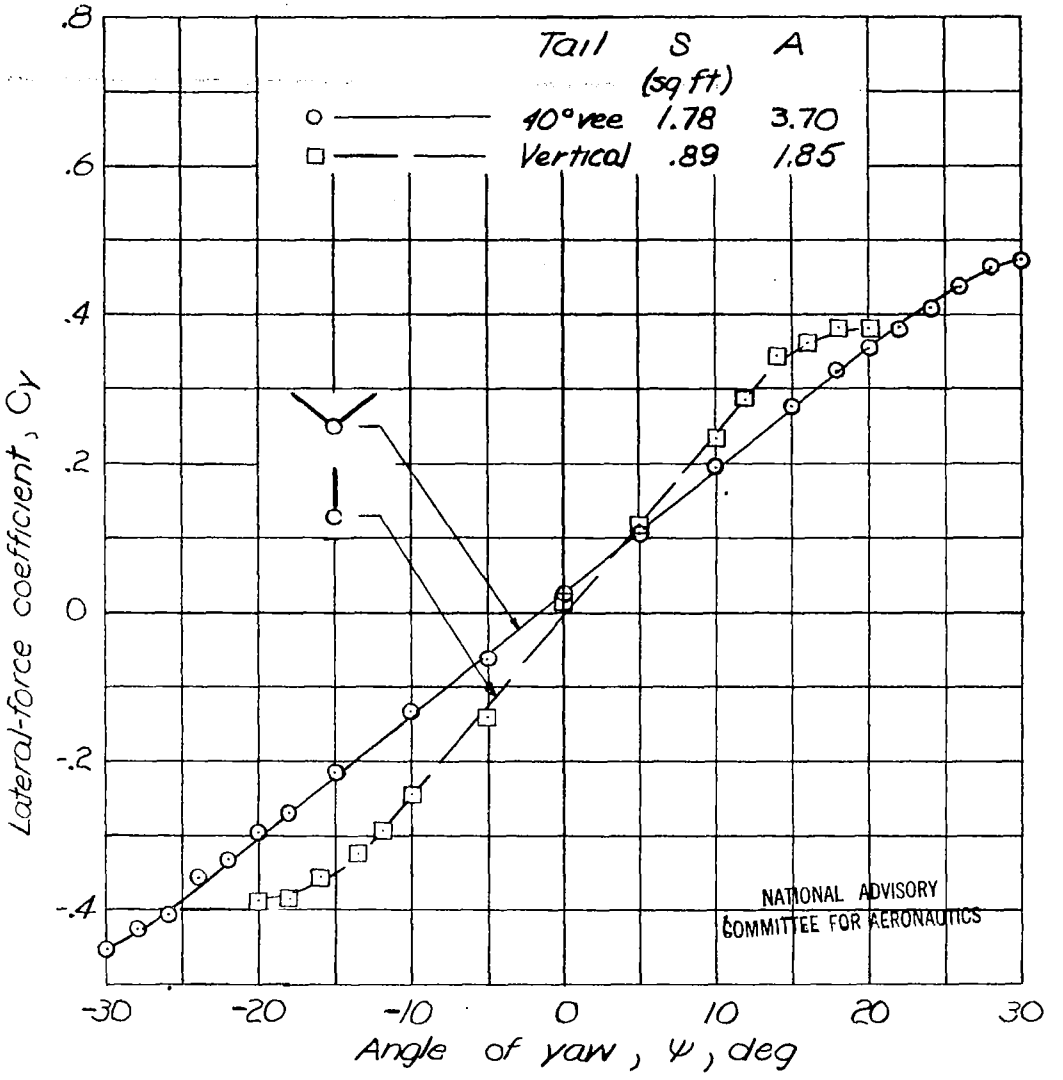

Figure 9.- Variation of tail lateral-force coefficient with angle of yaw for conventional vertical tail (single panel of tail surface B) and 40° vee tail (tail surface B). $\lambda = 0.56$. (Coefficients for both vertical and vee tails are based on area, span, and mean chord of complete tail surface B.)

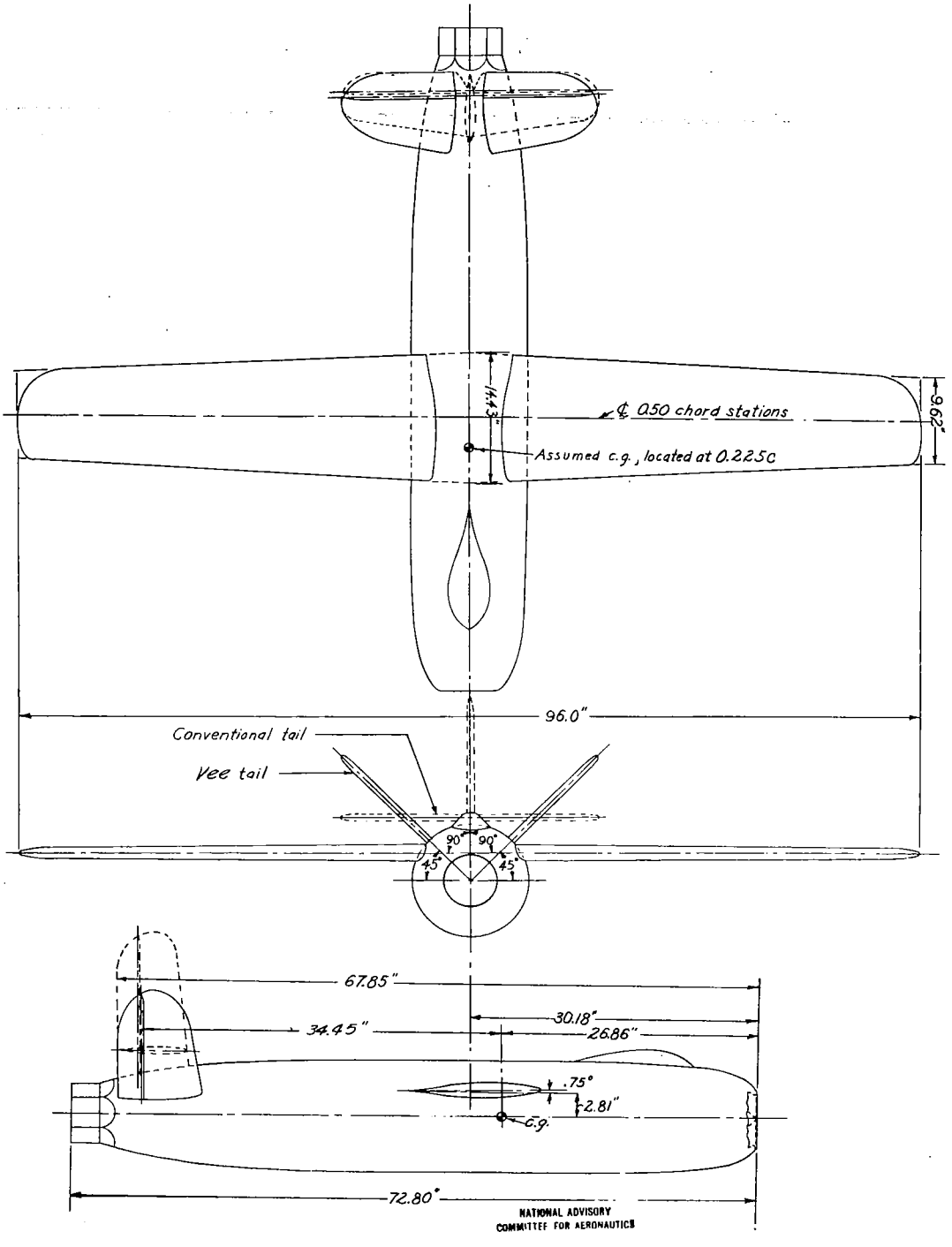

Figure 10.- Complete model with vee tail tested in Langley 7- by 10-foot tunnel. Wing area = 8.025 square feet.

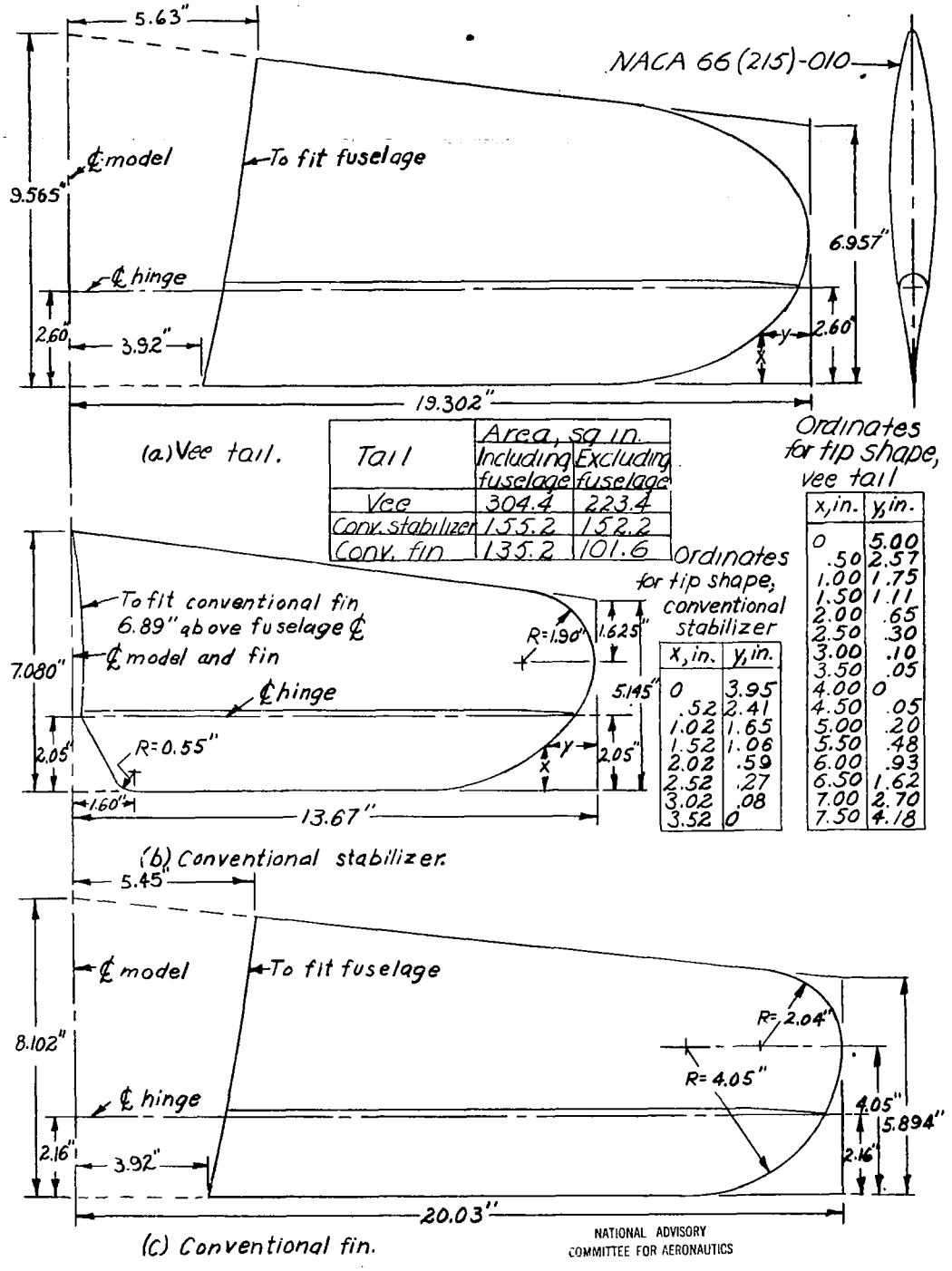

Figure 11.- Conventional tail and vee-tail surfaces tested on complete model in Langley 7-by 10-foot tunnel.

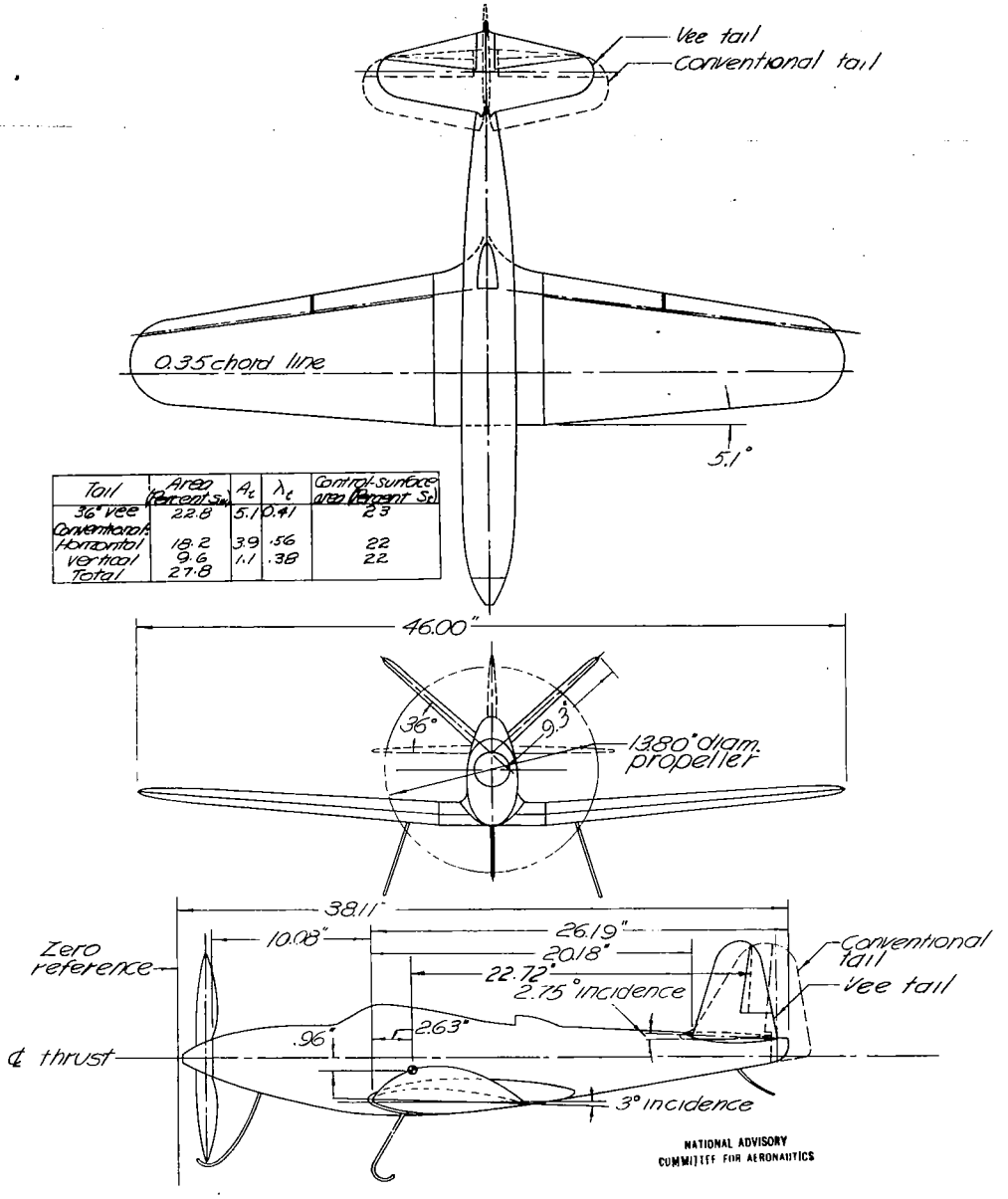

Tail	Area (Percent S_W)	A_t	λ_t	Control-surface area (Percent S_t)
36° Vee	22.8	5.1	0.41	23
Conventional:				
Horizontal	19.2	3.9	.56	22
Vertical	9.6	1.1	.38	22
Total	27.8			

Figure 12.- The $\frac{1}{10}$-scale model of fighter airplane with vee tail and conventional tails tested in Langley free-flight tunnel. Wing area = 2.48 square feet.

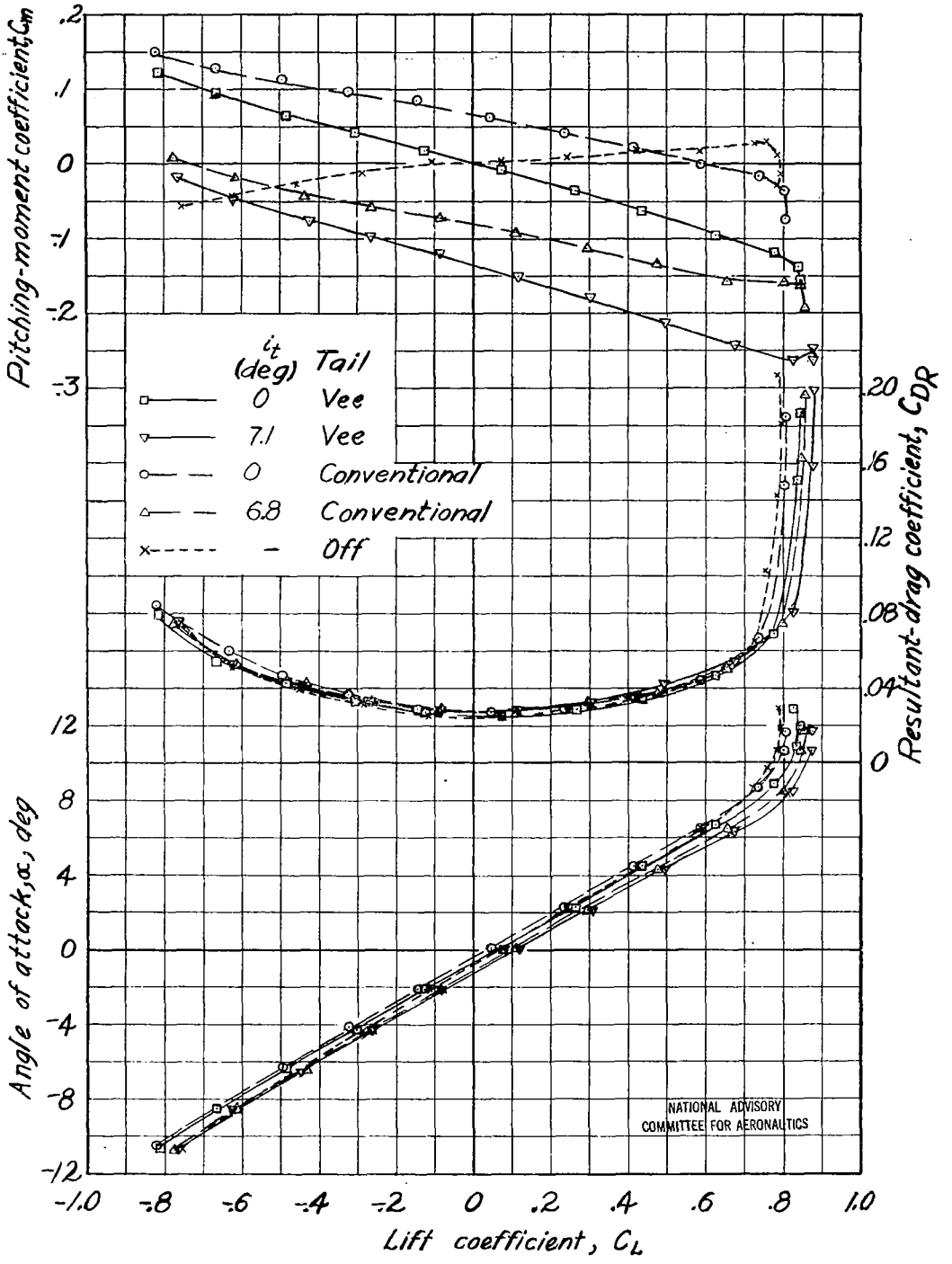

Figure 13.– Effect of vee and conventional tail surfaces on aerodynamic characteristics in pitch of a complete airplane model tested in the Langley 7-by 10-foot tunnel. $(\delta_e)_h = (\delta_e)_{vee} = \delta_r = 0°$.

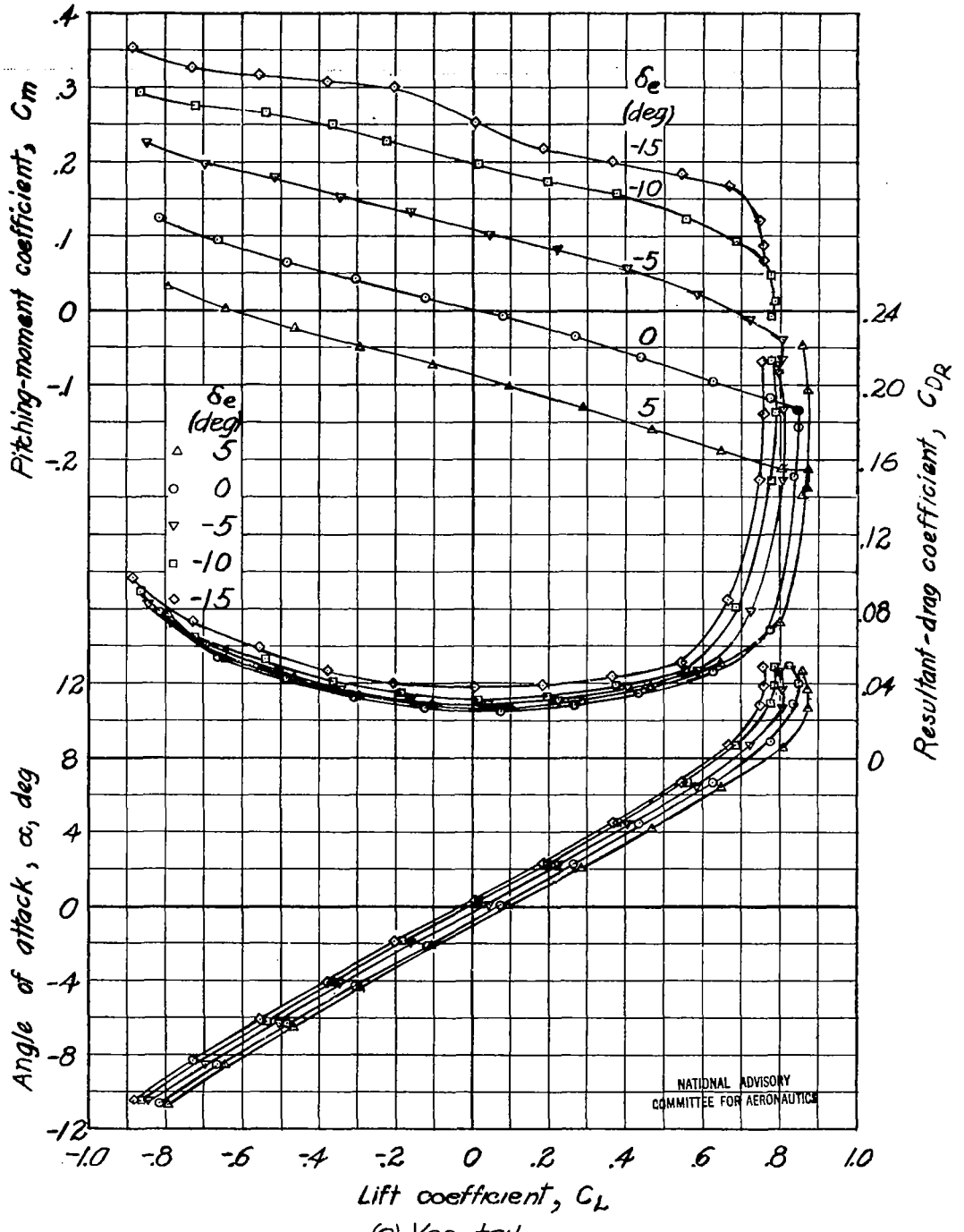

(a) Vee tail.

Figure 14.- Effect of elevator deflection on aerodynamic characteristics in pitch of a complete airplane model tested in the Langley 7-by 10-foot tunnel. $(i_t)_h = (i_t)_{vee} = 0°$.

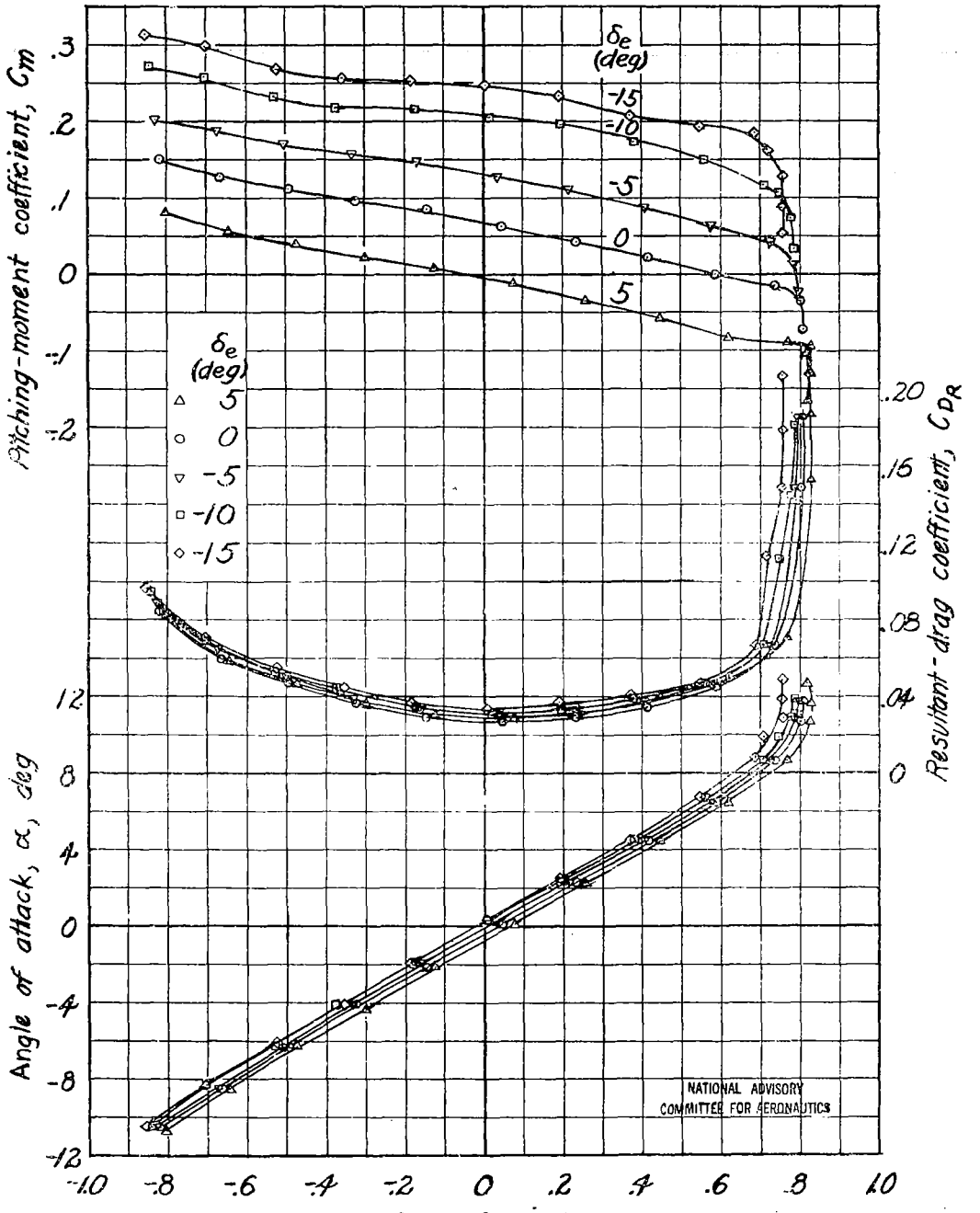

(b) Conventional tail.

Figure 14.-Concluded.

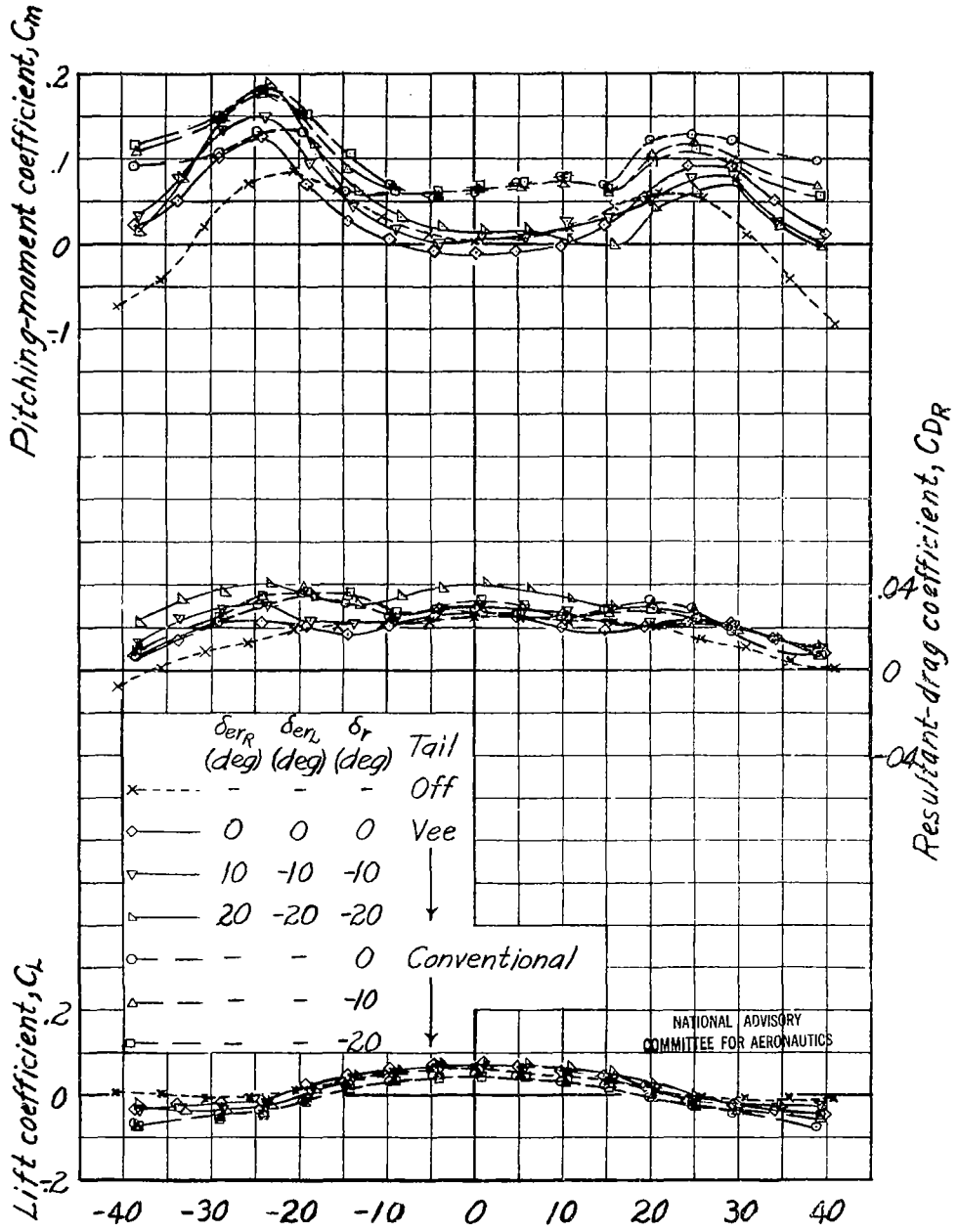

(a) $\alpha = 0.1°$; $\delta_e = 0°$.

Figure 15.- Comparative rudder effectiveness and aerodynamic characteristics in yaw for an airplane model with no tail, a vee tail, and a conventional tail. $(i_t)_n = (i_t)_{vee} = 0°$. Langley 7-by 10-foot tunnel.

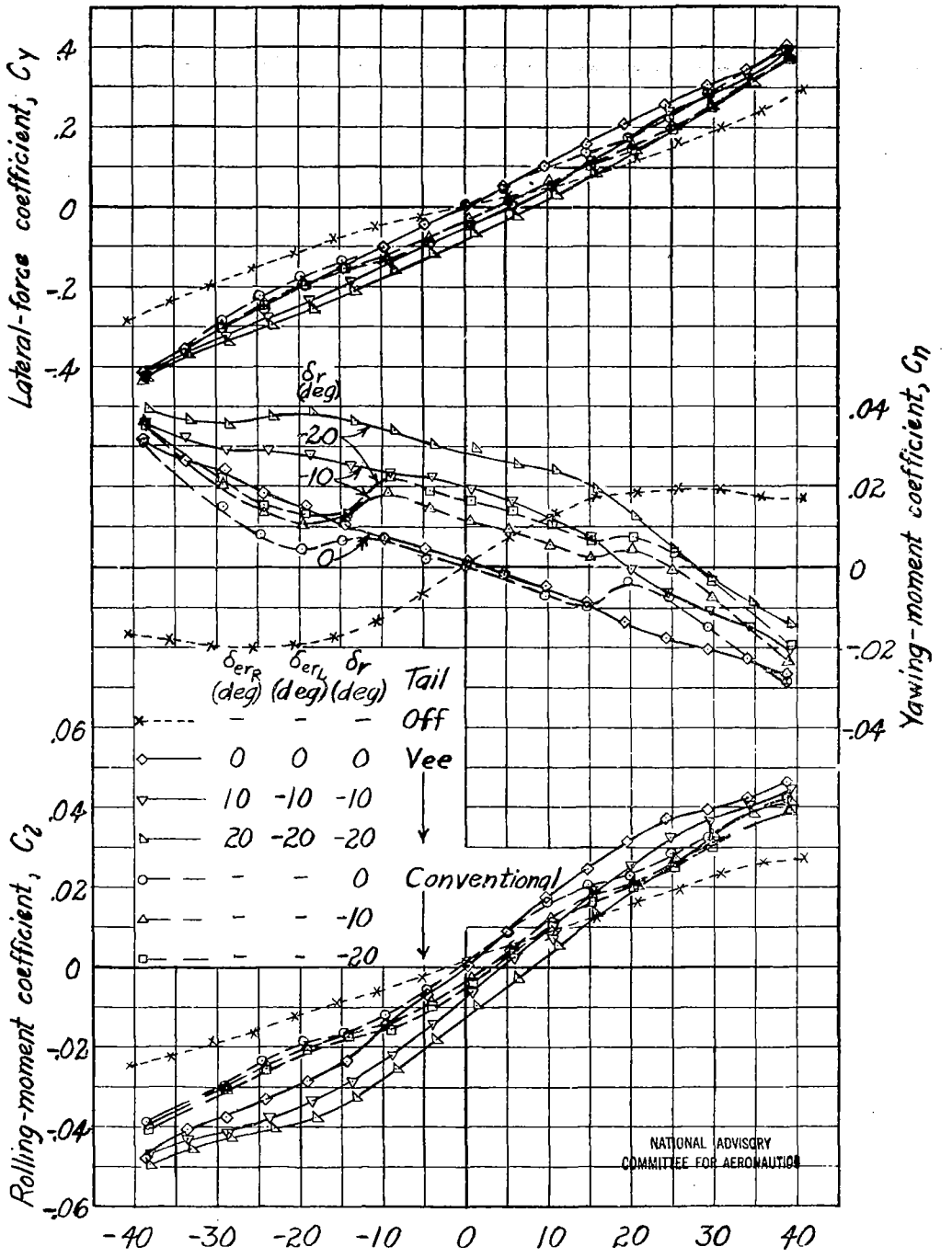

(a) $\alpha = 0.1°$; $d_e = 0°$. Concluded.

Figure 15.- Continued.

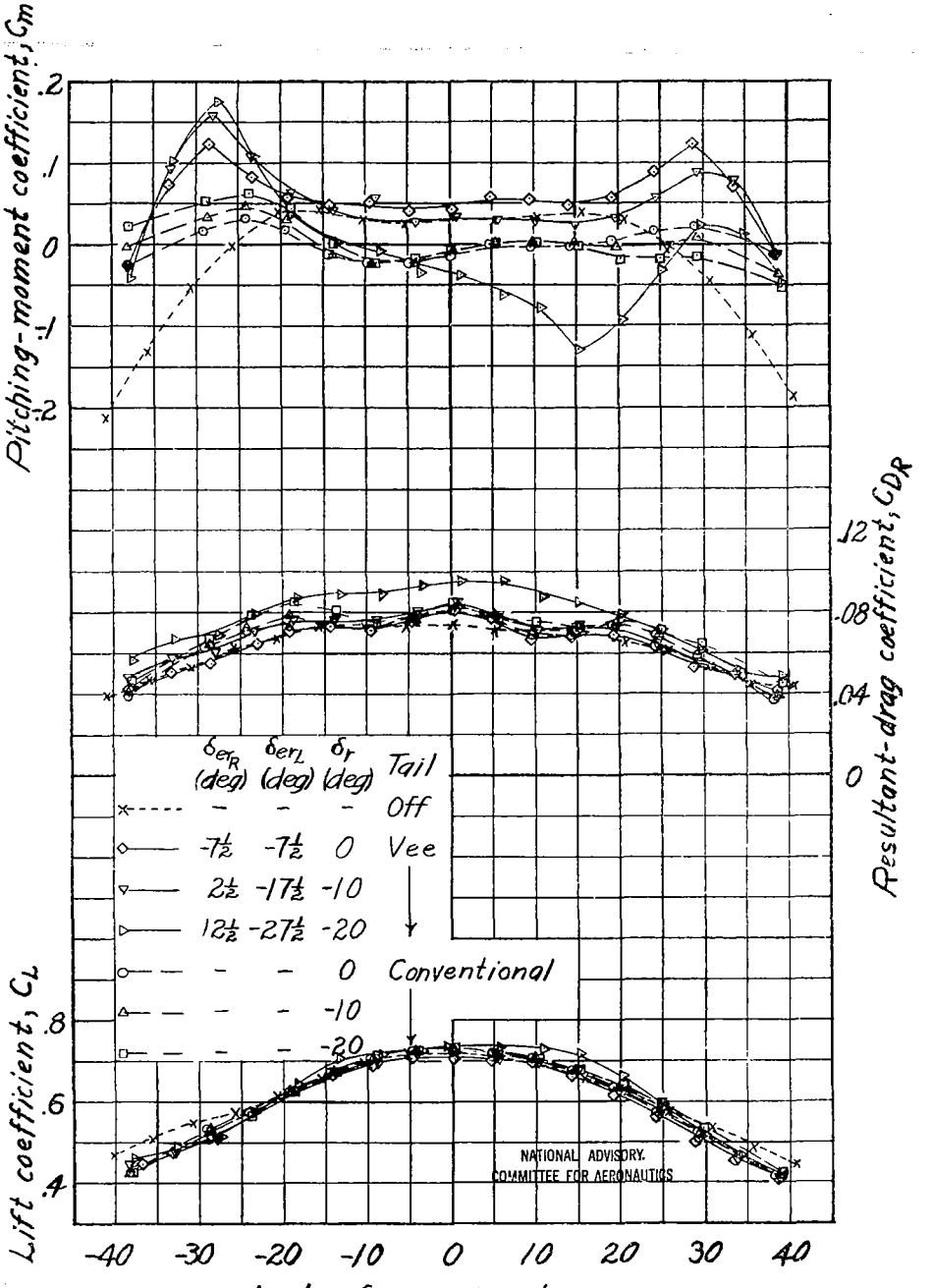

(b) $\alpha = 8.7°$; $(\delta_e)_n = 0°$; $(\delta_e)_{vee} = -7\frac{1}{2}°$.

Figure 15. - Continued.

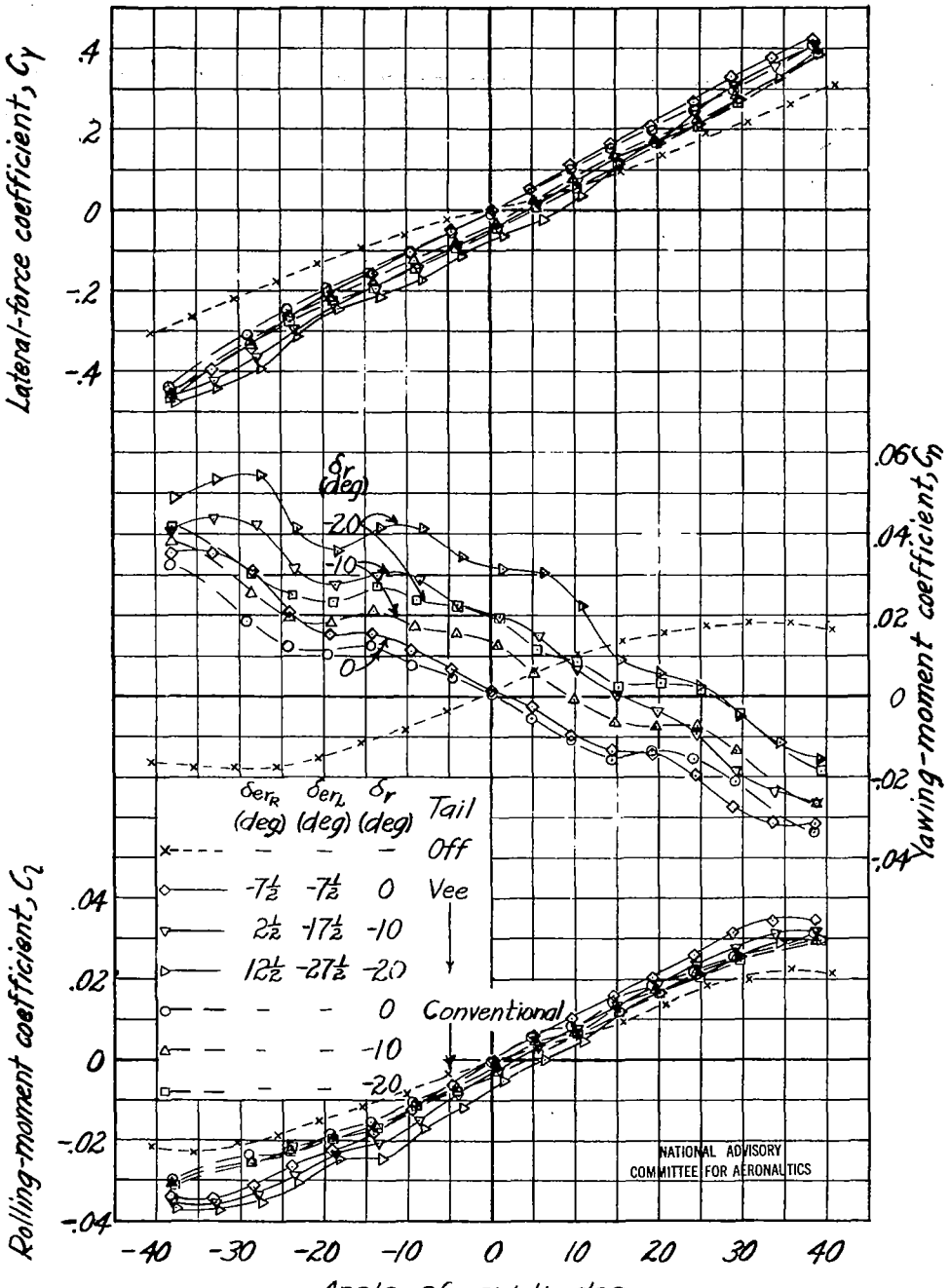

(b) $\alpha = 8.7°$; $(de)_h = 0°$; $(de)_{vee} = -7\frac{1}{2}°$. Concluded.

Figure 15. – Concluded.

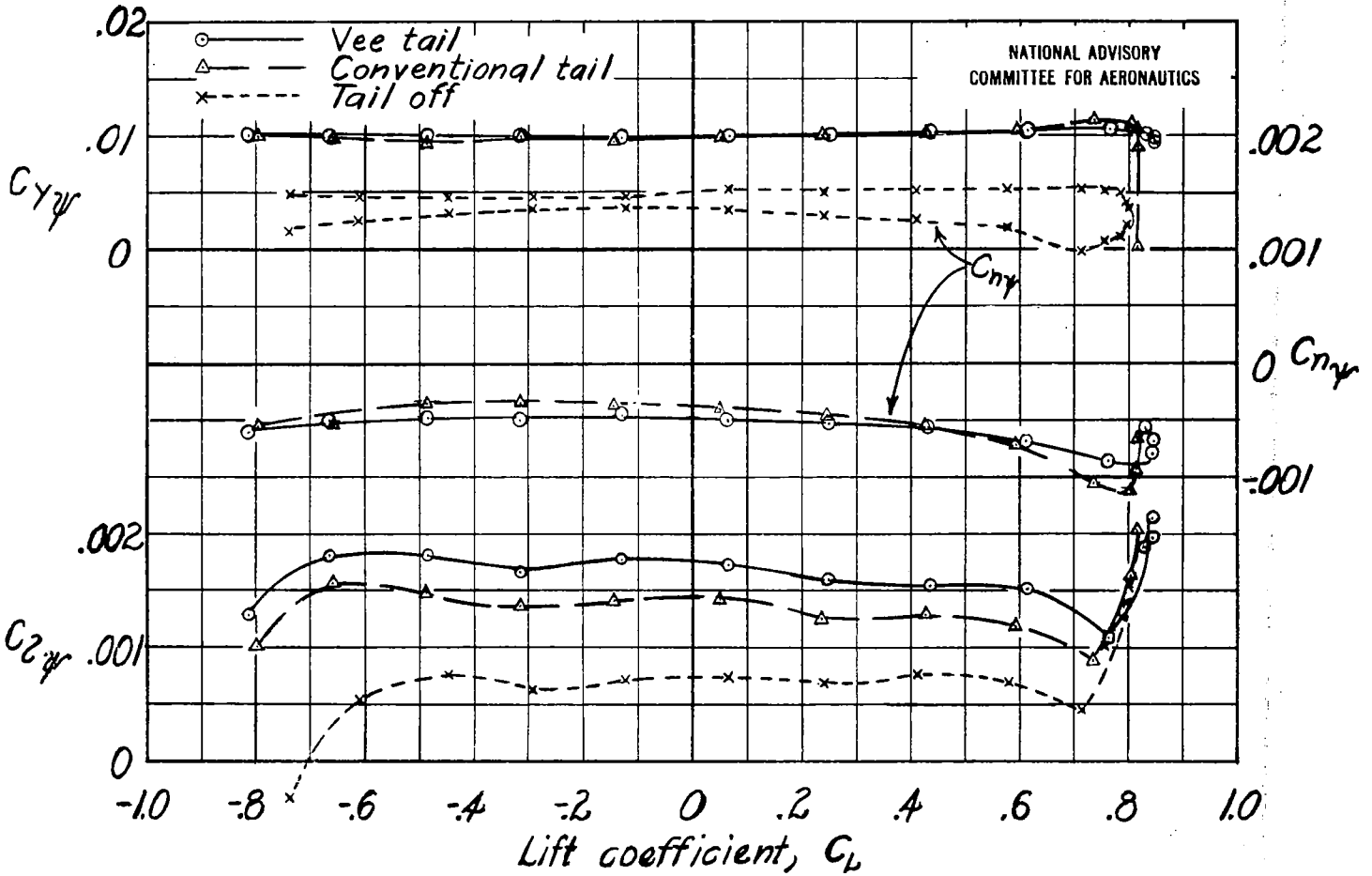

Figure 16.- Effect of a vee tail and a conventional tail on the variation of lateral-stability parameters with lift coefficient for an airplane model tested in the Langley 7- by 10-foot tunnel.

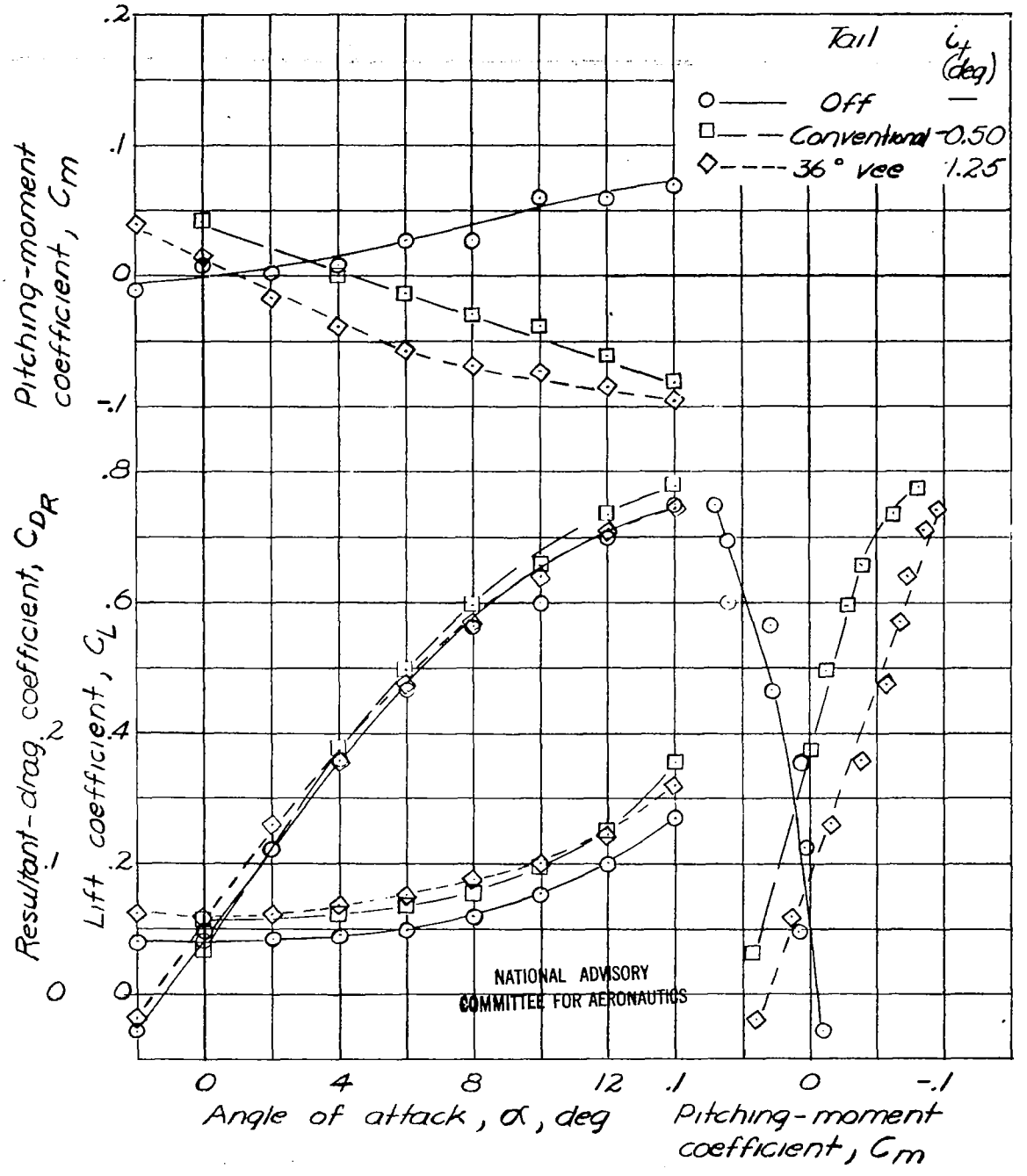

Figure 17.– Lift, drag, and pitching-moment characteristics of fighter-airplane model tested in the Langley free-flight tunnel. Flaps retracted; $T_c = 0$; $d_e = 0°$.

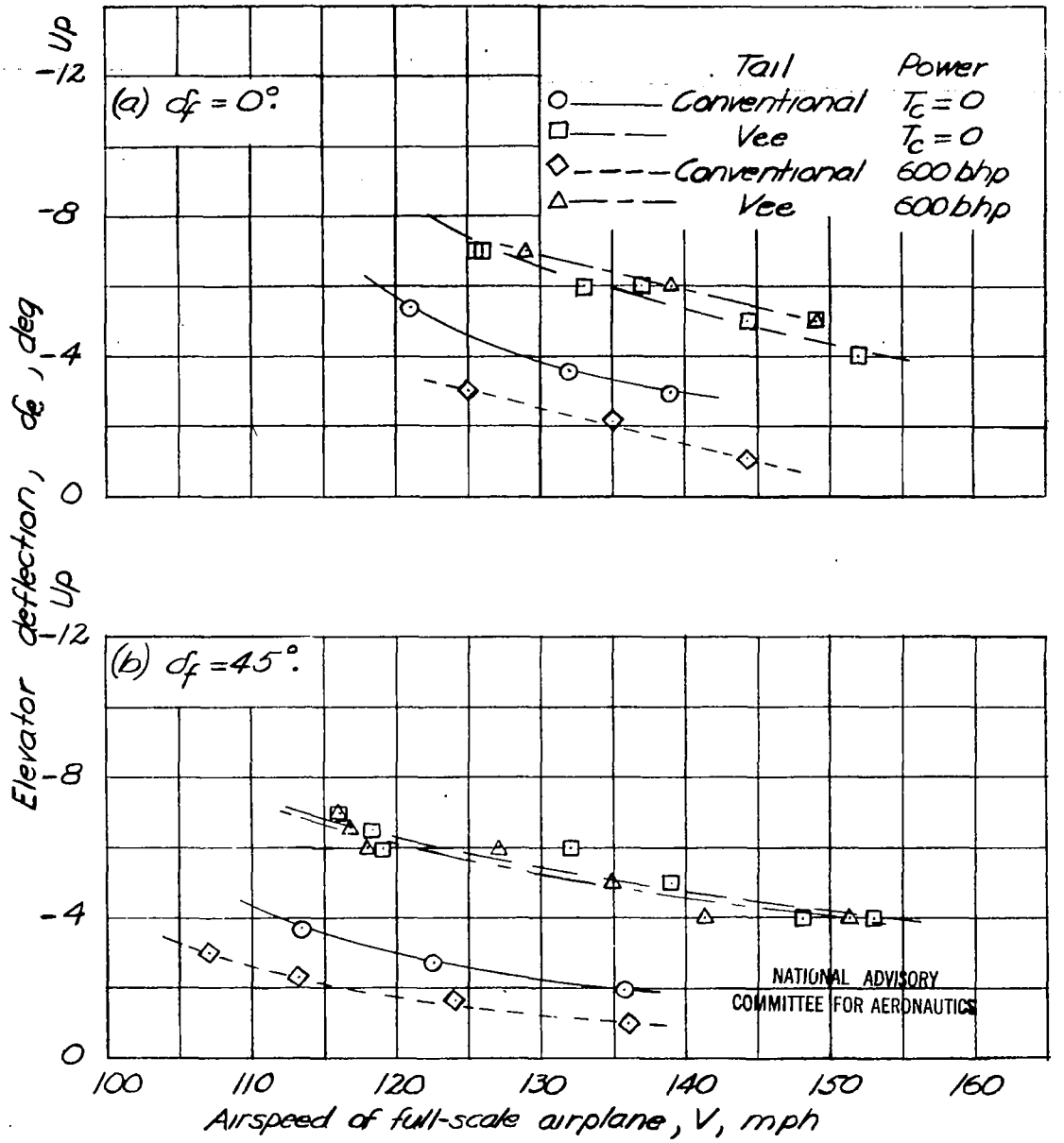

Figure 18.– Elevator deflections required to trim $\frac{1}{10}$-scale fighter-airplane model at various airspeeds with conventional and 36° vee tails. Tests made in Langley free-flight tunnel.

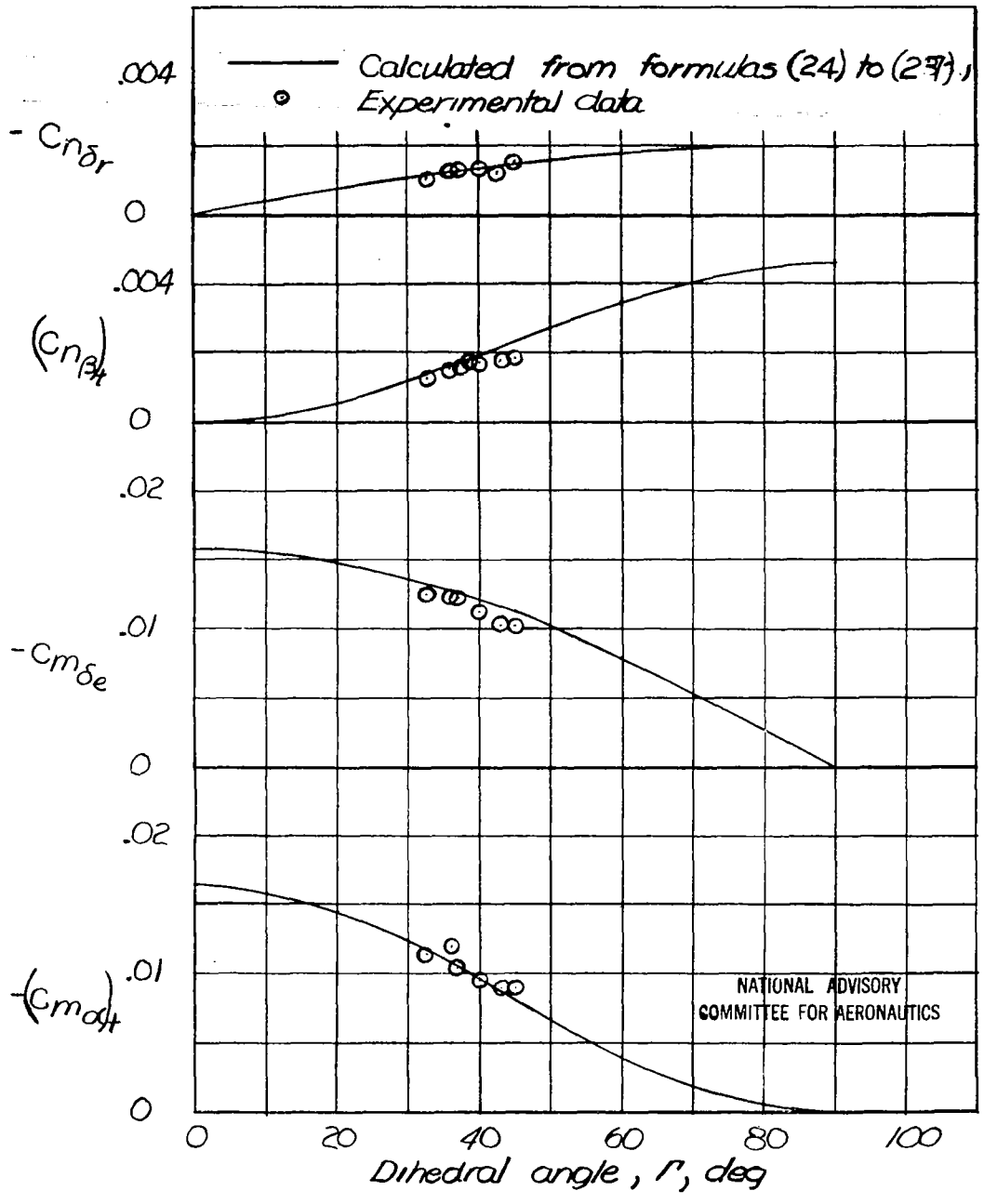

Figure 19.- Variation of vee-tail stability and control parameters with tail dihedral angle for fighter-airplane model tested in Langley free-flight tunnel.

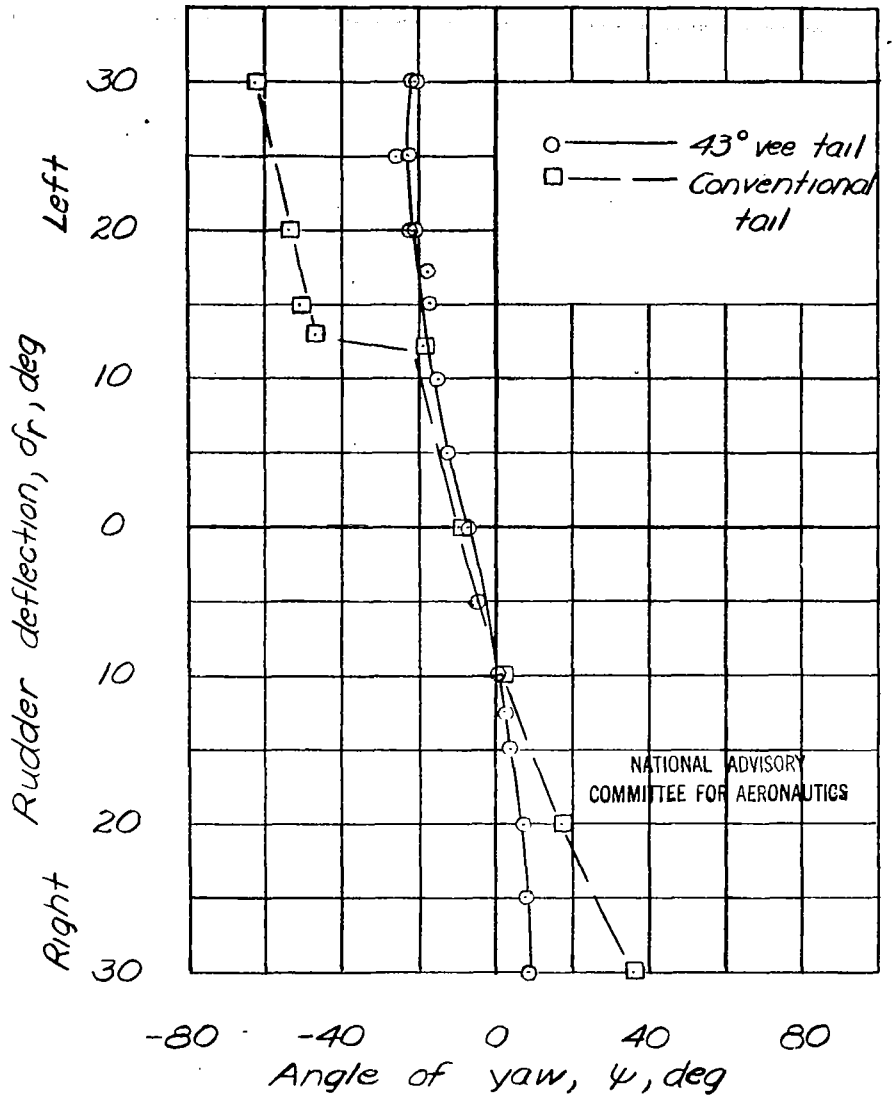

Figure 20.—Trim angles of yaw obtained with various rudder-pedal positions for the complete fighter-airplane model tested in the Langley free-flight tunnel with conventional and vee tails. Stick neutral; $\delta_f = 0°$; $\alpha = 8°$; $q = 1.04$ pounds per square foot; $T_c = 0.52$.